Incoherent Distributed Sources Tracking Algorithm for Massive MIMO Systems

Hui Chen, Tianjing Wang, Wenxu Zhang, Feng Lian, Guanghua Zhang

***Abstract*—To address the time-varying direction-of-arrival (DOA) tracking problem of incoherently distributed (ID) signal sources for massive multiple-input multiple-output (MIMO) systems, which involves critical challenges of data association ambiguity and measurement uncertainty in dynamic environments, this work proposes a novel tracking algorithm for ID sources using the generalized labeled multi-Bernoulli (GLMB) filter and smoother. The algorithm first models ID sources using a uniform rectangular array (URA), and then estimates the nominal DOA, along with angular spreads, via the beamspace unitary estimating signal parameters via rotational invariance techniques (UESPRIT) algorithm. The above estimates are then used as pseudo-measurements for each time step within the GLMB filter and smoother to improve estimation accuracy. At the same time, for the uncertainty of measurement noise, Cramér-Rao bound (CRB) is used to approximate the covariance of measurement noise in the tracking process. Within the framework of the GLMB smoother, a forward filtering stage is performed to generate the association history as well as the trajectory information using the GLMB filter. Term trajectories and trajectory fragments are removed through the trajectory pruning operation. Next, the backward smoothing is applied to achieve the data association of the ID sources and the estimation of kinematic states. To verify the effectiveness of the proposed approach, Monte Carlo (MC) simulations are performed. The results confirm its superior DOA tracking capability, enhanced estimation accuracy, and high robustness.**

***Index Terms*—Massive MIMO systems, Incoherent distributed sources, Uniform rectangular array, Generalized labeled multi-Bernoulli filter, Generalized labeled multi-Bernoulli smoother.**

I. Introduction

MASSIVE multiple-input multiple-output (MIMO) has become a cornerstone technology in fifth-generation (5G) and beyond wireless communications, which offers a flexible trade-off between multi-path gain and diversity gain, and enhances the spectral efficiency of wireless networks [1]. Massive MIMO demonstrates significant potential in application domains where dynamic multi-source tracking is crucial, such as millimeter-wave communication systems (e.g., 5G New Radio and future 6G networks) and indoor/outdoor precision positioning services (including augmented reality navigation and intelligent transportation systems). It yield substantial improvements in both antenna gain and array processing capabilities, enabling more efficient wireless communications in multi-user and complex propagation environments. However, their performance is highly dependent on the accuracy of direction-of-arrival (DOA) estimation of incoming signals. In practical applications, the phenomenon of angular spreading becomes increasingly significant. This necessitates modeling signal sources as distributed sources rather than point sources. In addition, the dynamic characteristics of signal sources introduces additional uncertainties, further complicating the DOA estimation process. Therefore, precise estimation and tracking of DOA for multiple distributed sources becomes a critical challenge for ensuring reliable and efficient communication.

In such systems, the base station (BS) is typically equipped with a large-scale antenna array consisting of several hundred to several thousand elements, enabling simultaneous communication with dozens of user terminals (UTs) [2]. The high spatial degrees of freedom and large array aperture inherent in such systems provide an effective means to enhance accuracy without requiring additional hardware. To accommodate the physical constraints of BS deployments, a two-dimensional (2D) massive MIMO system is typically adopted, enabling a dense arrangement of antenna elements within the BS in reality [3]. Conventional DOA estimation systems typically adopt a point-source model, which assumes that each signal source radiates energy in a single, discrete direction, or that each scattering cluster contributes a single propagation path between the base station and the mobile station [4]. However, in practical wireless propagation environments, multipath effects including scattering, reflection, diffraction, and refraction can cause the source to diffuse outward at certain angles in space. This necessitates a shift from point-source models to distributed source models, which more accurately capture the spatial characteristics of signal propagation. It can be further divided into coherently distributed (CD) and incoherently distributed (ID) sources, corresponding to slowly and rapidly time-varying channels [5]. For instance, in cellular wireless systems, multi-path propagation causes signals to arrive at the antenna array through multiple paths with different angles of arrival. This results in angular dispersion and time-varying

This work is supported by the National Natural Science Foundation of China (62163023, 61873116), the Gansu Provincial Basic Research Innovation Group of China (25JRRA058), the Central Government's Funds for Guiding Local Science and Technology Development of China (25ZYJA040) and the Gansu Provincial Key Talent Project of China (2024RCXM86).

Chen Hui is the School of Automation and Electrical Engineering, Lanzhou University of Technology, Lanzhou 730050, China (e-mail: chenh@lut.edu.cn).

Wang Tianjing is the School of Automation and Electrical Engineering, Lanzhou University of Technology, Lanzhou 730050, China (e-mail: wangtj@lut.edu.cn).

Zhang Wenxu is the School of Automation and Electrical Engineering, Lanzhou University of Technology, Lanzhou 730050, China (e-mail: wenxuzhang@foxmail.com).

Lian Feng is the School of Automation Science and Engineering, Xi'an Jiaotong University, Xi'an 710049, China (e-mail: lianfeng1981@mail.xjtu.edu.cn).

Zhang Guanghua is the School of Automation Science and Engineering, Xi'an Jiaotong University, Xi'an 710049, China (e-mail: MichaelZgh@stu.xjtu.edu.cn).

channel characteristics, thereby making ID source modeling more appropriate.

Among existing 2D localization methods for ID sources, both the maximum likelihood method [6] and the least squares-based covariance matching method [7] exhibit performance close to the theoretical optimum. However, in massive MIMO systems, these methods suffer from high computational complexity due to the exhaustive spectral peak search process [8], as the computational cost increases exponentially with the number of antennas and the fineness of the parameter search grid making them impractical for real-time implementation. In contrast, the widely studied estimate signal parameters via rotational invariance techniques (ESPRIT) algorithm [9]–[14] offers significant computational complexity advantages. It avoids spectral searching entirely by constructing the signal subspace and exploiting its inherent rotational invariance to obtain a closed-form solution through solving a generalized eigenvalue problem, making it particularly suitable for real-time massive MIMO applications. This method primarily constructs the generalized array manifold (GAM) through first-order Taylor series expansion approximation of the array manifold (AM), then estimates the parameters by exploiting the subspace rotational invariance relationship. Another algorithms exploits the rotational invariance property in the beamspace domain and addresses ID sources by designing suitable beamforming matrices [15]–[19]. However, all the above algorithms assume that the UTs are located at fixed positions. In practice, UTs in massive MIMO systems usually vary dynamically. Moreover, multi-path transmission signals are composed of multiple single components with different frequencies, amplitudes, and delays, which are superimposed on each other and exhibit non-stationary characteristics. These characteristics introduce significant challenges for traditional algorithms, limiting their effectiveness in dynamic environments.

In recent years, DOA estimation for moving sources has emerged as a prominent research focus, and its fundamental challenge lies in the effective association of DOA estimates across consecutive time steps with their corresponding signal sources. Although the tracking of a single distributed source has been investigated in the literature [20]–[24], the tracking of multiple distributed signal sources remains largely unexplored, especially in the application of massive MIMO systems. Since multiple signal sources more accurately represent the signal transmission characteristics in massive MIMO systems, this work employs multi-target filters [25]–[30] and smoothers based on random finite set (RFS) statistics to track the dynamic evolution of multiple ID sources. Notably smoothers [31]–[37] demonstrate superior estimation accuracy compared to filters by integrating the a priori information from the filtering process to globally optimize the target's historical states. In particular, the generalized labeled multi-Bernoulli (GLMB) smoother is an advanced multi-target tracker based on RFS statistics, efficiently solving the association problem by assigning unique labels to each target and maintaining label continuity during Bayesian updates. This method ensures high precision in managing measurement uncertainty, false alarms, and track management, ultimately delivering accurate and complete trajectory estimates in complex and dynamic tracking scenarios. This work integrates the Beamspace-UESPRIT estimator into the GLMB filtering and smoothing framework, demonstrating a strong synergistic effect. The Beamspace-UESPRIT algorithm provides low-complexity, high-resolution DOA parameter estimation at each time step, generating a set of unassociated pseudo-measurements. However, it does not inherently address the critical challenge of temporal data association across consecutive observations. This issue is effectively resolved by the GLMB filter and smoother, an optimal multi-target tracking framework based on RFS theory, which excels in handling measurement origin uncertainty, false alarms, and track management. By feeding the pseudo-measurements from Beamspace-UESPRIT into the GLMB filter and smoother, eliminate the need for explicit data association and computationally expensive peak searching steps. This combined approach enables efficient and accurate trajectory estimation of multiple ID sources, making it particularly well-suited for real-time applications in massive MIMO systems. Therefore, this paper proposes the Beamspace-UESPRIT GLMB filter and smoother for parameter estimation of ID sources in a massive MIMO system. The Beamspace-UESPRIT algorithm, operating in a reduced-dimensional beamspace domain, significantly reduces computational complexity compared to its element-space counterpart.

For ID sources, the DOA parameters are estimated by the UESPRIT algorithm using beamspace GAM modeling, which exploits the existence of rotational invariance in two identical closely spaced subarrays approximation. The estimated parameters, which form pseudo-measurements (a common technique where the outputs of a parameter estimator, e.g., DOA estimates, are treated as equivalent measurement inputs for a tracking filter), using the Cramér-Rao bound (CRB) employed in place of the measurement noise covariance. Rather than using a fixed or empirically tuned covariance, the CRB supplies a theoretically justified lower bound on the estimation error under the assumed signal model and thus serves as a principled, time-varying proxy for pseudo-measurement reliability. Based on these pseudo-measurements, the system performs preliminary tracking using the GLMB filter, followed by smoothing processing to enhance trajectory accuracy. During the filtering process, trajectory pruning is also performed as a post-processing procedure. This operation eliminates spurious or unreliable trajectories and trajectory fragments based on specific criteria (including statistical weight and confidence) to maintain computational efficiency. This approach eliminates computationally intensive procedures such as spectral peak searching and angle matching, making it particularly suitable for real-time tracking of ID sources in wireless systems. Moreover, the proposed method demonstrates strong robustness in estimating both the nominal DOA and angular spread parameters of the ID sources.

The rest of the paper is organized as follows. Section II introduces the modeling of dynamic ID signal sources, the measurement model in beamspace, and the primary assumptions. Section III proposes an ID signal source DOA estimation method based on the GLMB filter. This approach incorporates the UESPRIT algorithm—a beam dimension reduction technique—into the GLMB filter, thereby addressing the challenge

of dynamic DOA tracking. Section IV proposes a GLMB smoother for multi ID signal sources algorithm. In Section V, the complexity analysis of the proposed algorithm is given. Simulation results and analysis are provided in Section VI. Finally, Section VII concludes the paper.

Notations: Lower-case (upper-case) boldface characters denote vectors (matrices). The superscripts $*$, T, H, and $\dagger$ represent the conjugate, transpose, conjugate transpose, and pseudoinverse, respectively. $E\{\cdot\}$ denotes the statistical expectation. I_K is the $K \times K$ identity matrix, and $O_{M\times N}$ is the $M \times N$ zero matrix. $[\cdot]_{m,n}$ and $[\cdot]_m$ denote the (m,n)th entry of a matrix and the mth element of a vector, respectively. $\mathrm{diag}(\cdot)$ constructs a diagonal matrix from the elements in parentheses, and $\mathrm{blkdiag}(\cdot)$ forms a block diagonal matrix from the submatrices provided. $\mathrm{tr}(\cdot)$ and $\|\cdot\|_F$ are the trace and Frobenius norm of a matrix, respectively. $\odot$ denotes the Hadamard product. The imaginary unit is represented by i, and $\delta(\cdot)$ is the Kronecker delta function.

II. Signal Model For Massive Mimo Systems

A. Dynamic ID signal sources modeling

In this paper, a RFS is employed to model an ID signal source with a random quantities and random states, where X_t denotes the random process of the ID signal source. The array observation comprises point sources propagating through multiple paths and noise, collectively forming the ID signal source. The URA is configured at the BS of a 2D massive MIMO System and consists of $M = M_x M_y$ antenna elements, where M_x and M_y denote the number of antennas along the x-direction and y-direction. Suppose that uncorrelated narrowband ID sources transmitted by UEs impinge upon the URA at the BS. The schematic diagram of the propagation process is shown in Fig. 1. Set θ_t and ϕ_t as the DOA parameters of the ID signal source, and $\dot{\theta}_t$ and $\dot{\phi}_t$ as its movement velocity. Then, at time t, the state of the ID signal source is represented as $X_t = \{\mathbf{x}_t^1, \mathbf{x}_t^2, \cdots, \mathbf{x}_t^K\}$, $\mathbf{x}_t^i = \left[\theta_t^i, \dot{\theta}_t^i, \phi_t^i, \dot{\phi}_t^i\right]^{\mathrm{T}}$. Assuming the ID signal source evolves according to a linear state equation:

$$\mathbf{x}_{t+1} = F\mathbf{x}_t + G \tag{1}$$

$$F = \begin{bmatrix} 1 & 0 & t & 0 \\ 0 & 1 & 0 & t \\ 0 & 0 & 1 & 0 \\ 0 & 0 & 0 & 1 \end{bmatrix} \tag{2}$$

$$G_t = \begin{bmatrix} \Delta T^2/2 & 0 \\ \Delta T & 0 \\ 0 & \Delta T^2/2 \\ 0 & \Delta T \end{bmatrix} \tag{3}$$

here, F is the state transition matrix, describing the evolution of the target state over time. $\mathbf{x_t}$ represents the target state vector at time t. The process noise covariance matrix is denoted as $Q = diag\left(\sigma_v^2 G_t\right)$. The observed signal received at t can be denoted as follows [17]:

$$\mathbf{y}(t) = \sum_{k=1}^{K} s_k(t) \sum_{l=1}^{L_k} \gamma_{k,l}(t)\mathbf{a}(\theta_{k,l}(t), \phi_{k,l}(t)) + \mathbf{n}(t) \tag{4}$$

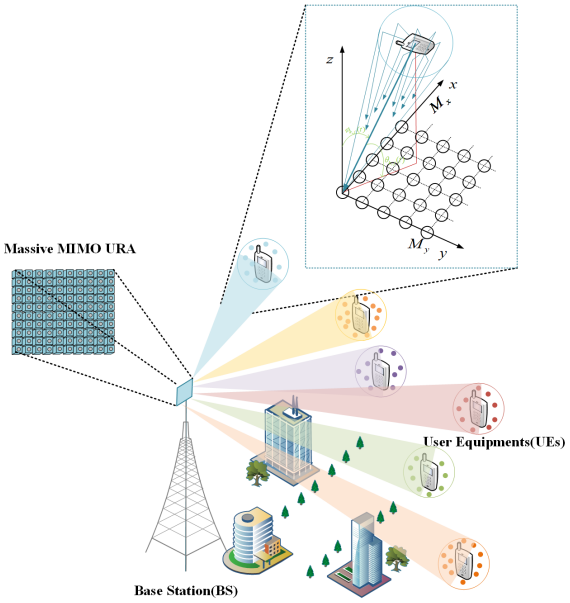

Fig. 1. Schematic diagram of ID sources propagation for Massive MIMO System.

where, $s_k(t)$ is the complex-valued signal transmitted by the kth UE, $t = 1, 2, \cdots, N$ is the sampling time, and N is the number of snapshots. The coefficient $\gamma_{k,l}$ denotes the complex-valued gain, and L_k is the number of rays inside the kth UE. The parameters $\theta_{k,l}(t)$ and $\phi_{k,l}(t)$ are the azimuth and elevation DOAs of the lth ray from the kth UE, respectively. The term $\mathbf{n}(t)$ denotes complex-valued additive noise with zero mean and variance σ_n^2. The matrix $\mathbf{a}(\theta_{k,l}(t), \phi_{k,l}(t))$ denotes the AM. The mth element element of the AM vector with respect to the origin element is expressed as: [17]:

$$\begin{aligned}[\mathbf{a}(\theta_{k,l}(t), \phi_{k,l}(t))]_m = \exp(ju\sin(\phi_{k,l}(t))[(m_x - 1) \\ \times \cos(\theta_{k,l}(t)) + (m_y - 1) \times \sin(\theta_{k,l}(t))])\end{aligned} \tag{5}$$

$$m = (m_y - 1)M_x + m_x \tag{6}$$

In the above equation, $u = 2\pi d/\lambda$, $m_x = 1, 2, \ldots, M_x$, $m_y = 1, 2, \ldots, M_y$, d denotes the antennas distance, and λ is the wavelength. The 2D DOAs can be expressed as follows:

$$\theta_{k,l}(t) = \bar{\theta}_k + \tilde{\theta}_{k,l}(t); \phi_{k,l}(t) = \bar{\phi}_k + \tilde{\phi}_{k,l}(t) \tag{7}$$

In the above equation, $\bar{\theta}_k$ and $\bar{\phi}_k$ are the real-valued nominal azimuth and elevation DOA. $\tilde{\theta}_{k,l}(t)$ and $\tilde{\phi}_{k,l}(t)$ are the corresponding angular deviations.

The formulation of the proposed method relies on the following assumptions [17]. Some initial assumptions are shown in Table I.

The transmitted signals, angular deviations, ray gains, and noise are assumed to be mutually uncorrelated.

The UEs are situated in a small-angle scattering environment, with a large number of paths for any ID source.

B. Beamspace signal sources measurement model

In the massive MIMO scenario, the diffusion range of the ID signal source is very small, and under small-angle expansion

TABLE I
INITIAL ASSUMPTIONS

Description	Formula
Angular deviations	$E\{\tilde{\theta}_{k,l}(t)\tilde{\theta}_{k',l'}(t')\} = \sigma^2_{\theta_k}\delta(k-k')\delta(l-l')\delta(t-t')$
Angular deviations	$E\{\tilde{\phi}_{k,l}(t)\tilde{\phi}_{k',l'}(t')\} = \sigma^2_{\phi_k}\delta(k-k')\delta(l-l')\delta(t-t')$
Path gains	$E\left\{\gamma_{k,j}(t)\,\gamma^*_{\tilde{k},\tilde{j}}(\tilde{t})\right\} = \frac{\sigma^2_{\gamma_k}}{N_k}\delta\left(k-\tilde{k}\right)\delta(j-\tilde{j})\,\delta(t-\tilde{t})$
Noise	$E\left\{\mathbf{n}(t)\,\mathbf{n}^{\mathrm{H}}(\tilde{t})\right\} = \sigma_n^2\mathbf{I}_M\delta(t-\tilde{t})$
Transmitted signals	$S_k = \lvert s_k(t)\rvert^2$

conditions, $\mathbf{a}(\theta_{k,l}(t),\phi_{k,l}(t))$ is approximated using a first-order Taylor expansion about the 2D nominal DOAs [17]:

$$\begin{aligned}&\mathbf{a}(\theta_{k,l}(t),\phi_{k,l}(t)) = \mathbf{a}(\bar{\theta}_k+\tilde{\theta}_{k,l}(t),\bar{\phi}_k+\tilde{\phi}_{k,l}(t))\\&\approx \mathbf{a}(\bar{\theta}_k,\bar{\phi}_k)+\frac{\partial\mathbf{a}(\bar{\theta}_k,\bar{\phi}_k)}{\partial\bar{\theta}_k}\tilde{\theta}_{k,l}(t)+\frac{\partial\mathbf{a}(\bar{\theta}_k,\bar{\phi}_k)}{\partial\bar{\phi}_k}\tilde{\phi}_{k,l}(t)\end{aligned} \tag{8}$$

The resulting received signal is formulated as:

$$\begin{aligned}\mathbf{y}(t)\approx\sum_{k=1}^{K}\Big(&\mathbf{a}(\theta_k,\phi_k)v_{k,1}(t)+\frac{\partial\mathbf{a}(\theta_k,\phi_k)}{\partial\theta_k}v_{k,2}(t)\\&+\frac{\mathbf{a}(\theta_k,\phi_k)}{\partial\phi_k}v_{k,3}(t)\Big)+\mathbf{n}(t)\in\mathbb{C}^{M\times1}\end{aligned} \tag{9}$$

Some of these parameters are expressed as follows:

$$\begin{cases}v_{k,1}(t)=s_k(t)\sum\limits_{l=1}^{L_k}\gamma_{k,l}(t)\\ v_{k,2}(t)=s_k(t)\sum\limits_{l=1}^{L_k}\gamma_{k,l}(t)\tilde{\theta}_{k,l}(t)\\ v_{k,3}(t)=s_k(t)\sum\limits_{l=1}^{L_k}\gamma_{k,l}(t)\tilde{\phi}_{k,l}(t)\end{cases} \tag{10}$$

The received signal is formulated in matrix representation as:

$$\mathbf{y}(t)\approx\mathbf{A}\mathbf{v}(t)+\mathbf{n}(t) \tag{11}$$

where:

$$\begin{aligned}\mathbf{A}=[&\mathbf{a}(\theta_1,\phi_1),\mathbf{a}(\theta_2,\phi_2),\ldots,\mathbf{a}(\theta_K,\phi_K),\\&\tfrac{\partial\mathbf{a}(\theta_1,\phi_1)}{\partial\theta_1},\tfrac{\partial\mathbf{a}(\theta_2,\phi_2)}{\partial\theta_2},\ldots,\tfrac{\partial\mathbf{a}(\theta_K,\phi_K)}{\partial\theta_K},\\&\tfrac{\partial\mathbf{a}(\theta_1,\phi_1)}{\partial\phi_1},\tfrac{\partial\mathbf{a}(\theta_2,\phi_2)}{\partial\phi_2},\ldots,\tfrac{\partial\mathbf{a}(\theta_K,\phi_K)}{\partial\phi_K}\Big]\in\mathbb{C}^{M\times3K}\end{aligned} \tag{12}$$

$$\begin{aligned}\mathbf{v}(t)=[&v_{1,1}(t),\ldots,v_{K,1}(t),v_{1,2}(t),\ldots,v_{K,2}(t),\\&v_{1,3}(t),\ldots,v_{K,3}(t)]^{\mathrm{T}}\in\mathbb{C}^{3K\times1}\end{aligned} \tag{13}$$

By partitioning the received signal matrix of URA along its columns, $\mathbf{y}(t)$ and $\mathbf{A}$ is formulated as, $i=1,2,\ldots,M_y$.

$$\mathbf{y}(t)=\left[\mathbf{y}_1^{\mathrm{T}}(t),\mathbf{y}_2^{\mathrm{T}}(t),\ldots,\mathbf{y}_{M_y}^{\mathrm{T}}(t)\right]^{\mathrm{T}} \tag{14}$$

$$\mathbf{y}_i(t)=[yy_{i,1}(t),y_{i,2}(t),\ldots,y_{i,M_y}(t)]^T\in\mathbb{C}^{M_y\times1} \tag{15}$$

$$\mathbf{A}=\left[\mathbf{A}_1^{\mathrm{T}},\mathbf{A}_2^{\mathrm{T}},\ldots,\mathbf{A}_{M_z}^{\mathrm{T}}\right]^{\mathrm{T}} \tag{16}$$

where $\mathbf{A}_i$ and $\mathbf{n}_i$ are the AM and noise vector of the ith column element. The received signals $\mathbf{y}_i(t)$ are then transformed into the beamspace domain [18].

$$\mathbf{z}_i(t)=\mathbf{W}^{\mathrm{H}}\mathbf{y}_i(t)=\mathbf{B}_i\mathbf{v}(t)+\mathbf{W}^{\mathrm{H}}\mathbf{n}_i(t)\in\mathbb{C}^{P\times1} \tag{17}$$

where $\mathbf{z}_i(t)$ is the beamspace measurements, $\mathbf{B}_i=\mathbf{W}^{\mathrm{H}}\mathbf{A}_i$ is the beamspace AM matrix, and $\mathbf{W}$ is the beamspace transformation matrix, which satisfies $\mathbf{W}^{\mathrm{H}}\mathbf{W}=\mathbf{I}_P$.

$$\mathbf{B}=\left[\mathbf{B}_1^{\mathrm{T}},\mathbf{B}_2^{\mathrm{T}},\ldots,\mathbf{B}_{M_z}^{\mathrm{T}}\right]^{\mathrm{T}}=\tilde{\mathbf{W}}^{\mathrm{H}}\mathbf{A}\in\mathbb{C}^{M_zP\times3K} \tag{18}$$

$$\tilde{\mathbf{W}}^{\mathrm{H}}=\mathrm{blkdiag}\left[\mathbf{W}^{\mathrm{H}},\ldots,\mathbf{W}^{\mathrm{H}}\right]\in\mathbb{C}^{PM_z\times M_yM_z} \tag{19}$$

The received beamspace reception measurement $\mathbf{z}(t)$ is formulated as:

$$\mathbf{z}(t)=\left[\mathbf{z}_1^{\mathrm{T}}(t),\mathbf{z}_2^{\mathrm{T}}(t),\ldots,\mathbf{z}_{M_z}^{\mathrm{T}}(t)\right]^{\mathrm{T}}=\tilde{\mathbf{W}}^{\mathrm{H}}\mathbf{y}(t)\in\mathbb{C}^{PM_z\times1} \tag{20}$$

III. GLMB FILTER FOR INCOHERENTLY DISTRIBUTED SOURCES

This section describes the process of tracking an ID signal source using a GLMB filter in a massive MIMO system. Based on the existing model, this paper further remodels the angle domain state within the framework of GLMB to adapt to the dynamic characteristics of multi-ID distributed signal sources. Compared with the traditional method of only single-time DOA estimation, our proposed modeling strategy realizes the systematic improvement from "static single-time estimation" to "continuous tracking of time series".

According to the distribution characteristics of ID signal sources in the spatial angle domain, we construct a state vector describing DOA and its time-varying evolution, and embed it into the prediction and update framework of GLMB. This state modeling enables the GLMB filter to dynamically estimate the spatial distribution of the ID signal source at each time step. This reformulated angle domain state model effectively solves the key problems of traditional ID estimation methods, such as the inability to handle cross-time data associations and the inability to capture angle time-varying.

In the process of constructing the measurement set, the measurements in this paper are constructed by the estimated results of the UESPRIT algorithm based on the URA array structure and the CRB approximation of the measurement noise covariance by estimating the error covariance. Specifically, we first use the UESPRIT algorithm to obtain the center angle and spread angle estimates of the target at the current time. These estimates are used as pseudo-measurements to input the GLMB filter at each time step, thereby achieving a preliminary capture of the spatial structure of the ID signal source.

Further, in order to quantify the statistical uncertainty of these pseudo-measurements, we introduce the CRB derived from the array signal model as the theoretical lower bound for the covariance of the estimation error, and use it to approximate the covariance matrix of the measurement noise. Because the CRB reflects the minimum variance that can be realized under the condition of known array structure, signal-to-noise ratio and snapshot number, this approximation has a clear theoretical basis in the simulation environment, and can provide a consistent and interpretable statistical description for the measurement model of GLMB without real noise statistical information.

A. Prediction step

The iterative process of the GLMB filter for incoherent distributed signal sources has a probability density similar to that of the GLMB filter, which is expressed as follows:

$$\pi(X)=\Delta(X)\sum_{(I,\xi)\in\mathcal{F}(\times\Xi)}w^{(I,\xi)}\delta_I[\mathcal{L}(X)][p^{(\cdot,\xi)}]^X \tag{21}$$

here, $X = \{(\mathbf{x},\mathbf{l})_i\},(i=1,2,\cdots,|X|)$ denotes the RFS label, $\Delta(X)$ represents the label indicator function, L denotes the discrete label space of ID signal sources, $\mathcal{F}()$ denotes the discrete trajectory set of ID signal sources, and Ξ denotes the discrete association space of ID signal sources. Each pair (I,ξ) represents an association hypothesis, $w^{(I,\xi)}$ denotes its corresponding weight, and $p^{(x,l;\xi)}$ denotes the probability density of a single target.

Assuming that the multi-ID signal sources has a prior distribution in the form of GLMB density, the probability density predicted by the multi-ID signal sources is represented as follows:

$$\pi(X)=\Delta(X)\sum_{(I,\xi)\in\mathcal{F}()\times\Xi} w^{(I,\xi)}\delta_I[\mathcal{L}(X)]\left[p^{(\cdot;\xi)}\right]^X \tag{22}$$

The specific parameter calculations are as follows:

$$w^{(I,\xi)}=w_B(I\cap\mathbb{B})\,w_S^{\xi}(I\cap\mathbb{L}) \tag{23}$$

$$\begin{aligned}p^{(\cdot;\xi)}=&\left\{1(l)\,\hat{w}_{S,i}^{(\xi)}(l),\mathbf{x}_{S,i}^{(\xi)}(l)\right\}_{i=1}^{J^{(\xi)}(l)}\\&\cup\left\{1(l)\,w_{B,i}^{(\xi)}(l),\mathbf{x}_{B,i}^{(\xi)}(l)\right\}_{i=1}^{B^{(\xi)}(l)}\end{aligned} \tag{24}$$

$$\mathbf{x}_{S,i}^{(\xi)}(l)\sim q\left(\cdot\mid\mathbf{x}_i^{(\xi)}(l),l,\mathbf{z}\right),i=1,\cdots,J^{(\xi)}(l) \tag{25}$$

$$w_{S,i}^{(\xi)}(l)=\frac{w_i^{(\xi)}(l)\,f\left(\mathbf{x}_{S,i}^{(\xi)}(l)\,|\mathbf{x}_i^{(\xi)}(l)\right)P_S\left(\mathbf{x}_i^{(\xi)}(l),l\right)}{q^{(\xi)}\left(\mathbf{x}_{S,i}^{(\xi)}(l)\,|\mathbf{x}_i^{(\xi)}(l),l,\mathbf{z}\right)} \tag{26}$$

$$\hat{w}_{S,i}^{(\xi)}(l)=w_{S,i}^{(\xi)}(l)\,/\sum\nolimits_{i=1}^{J^{(\xi)}(l)}w_{S,i}^{(\xi)}(l) \tag{27}$$

$$\mathbf{x}_{B,i}^{(\xi)}(l)\sim b(\cdot\mid\mathbf{z}),i=1,\cdots,B^{(\xi)}(l) \tag{28}$$

$$w_{B,i}^{(\xi)}(l)=p_B\left(\mathbf{x}_{B,i}^{(\xi)}\right)\Big/b\left(\mathbf{x}_{B,i}^{(\xi)}\mid\mathbf{z}\right) \tag{29}$$

Equation (23)-(29) details the calculation process for the multi-objective prediction weights and probability distribution. B is the ID signal source label space for newly generated sources; $p_B(\cdot,l)$ is the probability density of newly generated ID signal sources; $f(\mathbf{x}|\cdot,l)$ is the state transition function, and the labels of predicted surviving ID signal sources remain unchanged; $P_S(\cdot,l)$ is the ID signal sources survival probability.

B. Update step

1) Measurement modeling: In the GLMB filter for ID signal sources, the measurement model consists of two components: The received measurement and the measurement noise. In this work, the received measurements at each time step are modeled using the angle values of the ID signal sources, which are estimated via the UESPRIT algorithm. The measurement noise covariance is approximated by the CRB based on multiple ID signal sources. Firstly, the $\mathbf{R}_z$ is computed based on the beamspace measurements described above and its eigenvalue decomposition.

$$\begin{aligned}&\mathbf{R}_z=E\{\mathbf{z}(t)\mathbf{z}^{\mathrm{H}}(t)\}\\&=E\{\tilde{\mathbf{W}}^{\mathrm{H}}\mathbf{y}(t)\mathbf{y}^{\mathrm{H}}(t)\tilde{\mathbf{W}}\}=\mathbf{B}\mathbf{\Lambda}_v\mathbf{B}^{\mathrm{H}}+\sigma_n^2\mathbf{I}_{PM_z}\in\mathbb{C}^{PM_z\times PM_z}\end{aligned} \tag{30}$$

$$\mathbf{R}_z=\mathbf{U}_s\mathbf{\Sigma}_s\mathbf{U}_s^{\mathrm{H}}+\sigma_n^2\mathbf{U}_n\mathbf{U}_n^{\mathrm{H}} \tag{31}$$

where $\mathbf{U}_s\in\mathbb{C}^{PM_y\times 3K}$ and $\mathbf{U}_n\in\mathbb{C}^{PM_z\times(PM_z-3K)}$ represent the signal and noise subspaces of the beamspace, respectively, each composed of the corresponding eigenvectors.

Since the core of the UESPRIT algorithm is the rotation invariance between signal subspaces, it is assumed that there exists a matrix $\mathbf{Q}$ such that the beam subspaces satisfy a linear relationship, i.e., $\mathbf{Q}\mathrm{B}_i=\mathbf{Q}\mathbf{F}^{\mathrm{H}}\mathbf{B}_i\mathbf{\Phi}_1$ holds. Where,

$$\mathbf{\Phi}_1=\begin{bmatrix}\mathbf{\Lambda}_{1,1}&\mathbf{\Lambda}_{1,2}&\mathbf{\Lambda}_{1,3}\\\mathbf{0}_{K\times K}&\mathbf{\Lambda}_{1,1}&\mathbf{0}_{K\times K}\\\mathbf{0}_{K\times K}&\mathbf{0}_{K\times K}&\mathbf{\Lambda}_{1,1}\end{bmatrix} \tag{32}$$

$$\begin{aligned}&\mathbf{\Lambda}_{1,1}=\mathrm{diag}\left[H_1(\theta_1,\phi_1),\ldots,H_1(\theta_K,\phi_K)\right]\\&\mathbf{\Lambda}_{1,2}=\mathrm{diag}\left[\partial H_1(\theta_1,\phi_1)/\partial\theta_1,\ldots,\partial H_1(\theta_K,\phi_K)/\partial\theta_K\right]\\&\mathbf{\Lambda}_{1,3}=\mathrm{diag}\left[\partial H_1(\theta_1,\phi_1)/\partial\phi_1,\ldots,\partial H_1(\theta_K,\phi_K)/\partial\phi_K\right]\end{aligned} \tag{33}$$

$$H_1(\theta_k,\phi_k)=\exp\left(ju\sin(\phi_k)\cos(\theta_k)\right) \tag{34}$$

For an ID signal source, to establish a rotation-invariant structure for two-dimensional DOA estimation beam space, it is divided into the x-direction and y-direction. The beamforming matrix $\mathbf{W}$ is set as the standard discrete Fourier transform (DFT) matrix, denoted by $\mathbf{W}=\left[\mathbf{t}_1^{\mathrm{T}},\mathbf{t}_2^{\mathrm{T}},\cdots,\mathbf{t}_P^{\mathrm{T}}\right]$, $\mathbf{W}\in\mathbb{C}^{M_y\times P}$ $(P<M_y)$, $\mathbf{t}_p=[1,\exp(j2\pi p/M_x),\cdots,\exp(j2\pi p(M_x-1)/M_x)]$.

For the x-direction, first define the selection matrix $\mathbf{J}_1=\left[\begin{array}{cc}\mathbf{I}_{M_x-1}&\mathbf{0}_{(M_x-1)\times 1}\end{array}\right]$ and $\mathbf{J}_2=\left[\begin{array}{cc}\mathbf{0}_{(M_x-1)\times 1}&\mathbf{I}_{M_x-1}\end{array}\right]$. And it satisfies $\mathbf{J}_1\mathbf{W}=\mathbf{J}_2\mathbf{W}\mathbf{F}$. Where, $\mathbf{F}\in\mathbb{C}^{P\times P}$ is a nonsingular matrix. Then the linear transformation matrix:

$$\mathbf{F}=\mathrm{diag}\left[\exp(-j2\pi/M_x),\ldots,\exp(-j2\pi P/M_x)\right] \tag{35}$$

$$\mathbf{Q}=\mathbf{J}_Q\Gamma\in\mathbb{C}^{P\times P} \tag{36}$$

$$\begin{aligned}\Gamma=\mathrm{diag}&\left[\exp(j2\pi(M_x-1)/M_x),\cdots,\right.\\&\left.\exp(j2\pi P(M_x-1)/M_x)\right]\in\mathbb{C}^{P\times P}\end{aligned} \tag{37}$$

$$\mathbf{J}_Q=\begin{bmatrix}1&-1&\cdots&0&0\\0&1&-1&\cdots&0\\\vdots&\vdots&\ddots&\vdots&\vdots\\0&0&\cdots&1&-1\\0&0&\cdots&0&0\end{bmatrix}\in\mathbb{C}^{P\times P} \tag{38}$$

Therefore, when $i=1,2,\cdots,M_y$, get $\tilde{\mathbf{Q}}\mathbf{B}=\mathbf{\Omega}\mathbf{B}\mathbf{\Phi}_1$.

$$\tilde{\mathbf{Q}}=\mathrm{blkdiag}\left[\mathbf{Q},\mathbf{Q},\ldots,\mathbf{Q}\right]\in\mathbb{C}^{PM_y\times PM_y} \tag{39}$$

$$\mathbf{\Omega}=\mathrm{blkdiag}\left[\mathbf{Q}\mathbf{F}^{\mathrm{H}},\mathbf{Q}\mathbf{F}^{\mathrm{H}},\ldots,\mathbf{Q}\mathbf{F}^{\mathrm{H}}\right]\in\mathbb{C}^{PM_y\times PM_y} \tag{40}$$

For the y-direction, define the selection matrix $\mathbf{J}_3=\left[\mathbf{I}_{P(M_y-1)},\mathbf{0}_{P(M_y-1)\times P}\right]\in\mathbb{C}^{(PM_y-1)\times PM_y}$, $\mathbf{J}_4=\left[\mathbf{0}_{P(M_y-1)\times P},\mathbf{I}_{P(M_y-1)}\right]\in\mathbb{C}^{(PM_y-1)\times PM_y}$, and reconstruct the AM matrix.

$$\mathbf{b}_3(\theta_k,\phi_k)=\mathbf{J}_3\mathbf{b}(\theta_k,\phi_k) \tag{41}$$

$$\mathbf{b}_4(\theta_k,\phi_k)=H_2(\theta_k,\phi_k)\mathbf{b}_3(\theta_k,\phi_k) \tag{42}$$

$$\begin{aligned}&\frac{\partial\mathbf{b}_4(\theta_k,\phi_k)}{\partial\theta_k}=H_2(\theta_k,\phi_k)\frac{\partial\mathbf{b}_3(\theta_k,\phi_k)}{\partial\theta_k}\\&+\frac{\partial H_2(\theta_k,\phi_k)}{\partial\theta_k}\mathbf{b}_3(\theta_k,\phi_k)\end{aligned} \tag{43}$$

$$H_2(\theta_k,\phi_k)=\exp\left(ju\sin\left(\phi_k\right)\sin\left(\theta_k\right)\right) \tag{44}$$

here, $\mathbf{b}(\theta_k,\phi_k)=\tilde{\mathbf{W}}^{\mathrm{H}}\mathbf{a}(\theta_k,\phi_k)$ denotes the beamspace AM matrix. In summary, obtain the linear relationship $\mathbf{J}_4\mathbf{B}=\mathbf{J}_3\mathbf{B}\mathbf{\Phi}_2$.

$$\mathbf{\Phi}_2=\begin{bmatrix}\mathbf{\Lambda}_{2,1} & \mathbf{\Lambda}_{2,2} & \mathbf{\Lambda}_{2,3}\\ \mathbf{0}_{K\times K} & \mathbf{\Lambda}_{2,1} & \mathbf{0}_{K\times K}\\ \mathbf{0}_{K\times K} & \mathbf{0}_{K\times K} & \mathbf{\Lambda}_{2,1}\end{bmatrix} \tag{45}$$

$$\begin{aligned}\mathbf{\Lambda}_{2,1}&=\mathrm{diag}\left[H_2(\theta_1,\phi_1),\ldots,H_2(\theta_K,\phi_K)\right]\\ \mathbf{\Lambda}_{2,2}&=\mathrm{diag}\left[\partial H_2(\theta_1,\phi_1)/\partial\theta_1,\ldots,\partial H_2(\theta_K,\phi_K)/\partial\theta_K\right]\\ \mathbf{\Lambda}_{2,3}&=\mathrm{diag}\left[\partial H_2(\theta_1,\phi_1)/\partial\phi_1,\ldots,\partial H_2(\theta_K,\phi_K)/\partial\phi_K\right]\end{aligned} \tag{46}$$

Based on the relationship between $\mathbf{B}$ and $\mathbf{U}_s$, a rotational invariance relationship can be established between the subspaces of the beamspace signals.

$$\tilde{\mathbf{Q}}\mathbf{U}_s\mathbf{T}=\Omega\mathbf{U}_s\mathbf{T}\mathbf{\Phi}_1,\mathbf{J}_4\mathbf{U}_s\mathbf{T}=\mathbf{J}_3\mathbf{U}_s\mathbf{T}\mathbf{\Phi}_2 \tag{47}$$

$$\tilde{\mathbf{Q}}\mathbf{U}_s=\Omega\mathbf{U}_s\mathbf{T}\mathbf{\Phi}_1\mathbf{T}^{-1}=\Omega\mathbf{U}_s\mathbf{\Psi}_1 \tag{48}$$

$$\mathbf{J}_4\mathbf{U}_s=\mathbf{J}_3\mathbf{U}_s\mathbf{T}\mathbf{\Phi}_2\mathbf{T}^{-1}=\mathbf{J}_3\mathbf{U}_s\mathbf{\Psi}_2 \tag{49}$$

Since $\mathbf{U}_s$ is derived from observations, the Total Least Squares (TLS) criterion is employed to compute the eigenvalues of $\mathbf{\Psi}_1$ and $\mathbf{\Psi}_2$ [17], which are associated with the nominal DOA. The detailed computational procedure is described below.

The explicit forms of $\mathbf{F}_x$ and $\mathbf{F}_y$ are as follows:

$$\mathbf{F}_x=\left[\Omega\mathbf{U}_s,\tilde{\mathbf{Q}}\mathbf{U}_s\right]^{\mathrm{H}}\left[\Omega\mathbf{U}_s,\tilde{\mathbf{Q}}\mathbf{U}_s\right] \tag{50}$$

$$\mathbf{F}_y=\left[\mathbf{J}_3\mathbf{U}_s,\mathbf{J}_4\mathbf{U}_s\right]^{\mathrm{H}}\left[\mathbf{J}_3\mathbf{U}_s,\mathbf{J}_4\mathbf{U}_s\right] \tag{51}$$

Algorithm 1 Matching of the Eigenvalues.

Calculate the EVD of $\hat{\mathbf{\Psi}}_1$ and $\hat{\mathbf{\Psi}}_2$;
Define $\hat{\mathbf{\Psi}}_3=\hat{\mathbf{\Psi}}_1\hat{\mathbf{\Psi}}_2$ and $\hat{\mathbf{\Psi}}_4=\hat{\mathbf{\Psi}}_1\hat{\mathbf{\Psi}}_2^{-1}$, and calculate the EVD of $\hat{\mathbf{\Psi}}_3$:$\hat{\mathbf{\Psi}}_3=\hat{\mathbf{\Psi}}_1\hat{\mathbf{\Psi}}_2\approx\mathbf{T}\mathbf{\Phi}_{2,1}\mathbf{\Phi}_{3,1}\mathbf{T}^{-1}=\mathbf{T}_3\mathbf{\Lambda}_3\mathbf{T}_3^{-1}$
$\hat{\mathbf{\Psi}}_4=\hat{\mathbf{\Psi}}_1\hat{\mathbf{\Psi}}_2^{-1}{}_2\approx\mathbf{T}\mathbf{\Phi}_{2,1}\mathbf{\Phi}_{3,1}^{-1}\mathbf{T}^{-1}$;
Hence obtaining $\mathbf{\Lambda}_3=\mathbf{T}_3^{-1}\hat{\mathbf{\Psi}}_3\mathbf{T}_3\approx\mathbf{T}_3^{-1}\mathbf{T}\mathbf{\Phi}_{2,1}\mathbf{\Phi}_{3,1}\mathbf{T}^{-1}\mathbf{T}_3$;
Calculate $\tilde{\mathbf{\Psi}}_4$:$\tilde{\mathbf{\Psi}}_4=\mathbf{T}_3^{-1}\hat{\mathbf{\Psi}}_4\mathbf{T}_3\approx\mathbf{T}_3^{-1}\mathbf{T}\mathbf{\Phi}_{2,1}\mathbf{\Phi}_{3,1}^{-1}\mathbf{T}^{-1}\mathbf{T}_3$;
for $p=1:3K$
  $p=p+1$;
  Calculate $\beta_{p,\tilde{p},1}$ and $\beta_{p,\tilde{p},2}$;
  Match $\beta_{p,\tilde{p},1}$ and $[\mathbf{\Lambda}_3]_{p',p'}$, $\beta_{p,\tilde{p},2}$ and $\left[\tilde{\mathbf{\Psi}}_4\right]_{p',p'}$;
  Find the corresponding relation between $\mathbf{\Lambda}_1$ and $\mathbf{\Lambda}_2$;
  Calculate $\left[\tilde{\mathbf{\Lambda}}_2\right]_{p,p}=[\mathbf{\Lambda}_2]_{x_p,x_p}$;
end
The diagonal entries of $\mathbf{\Lambda}_1$ are ordered in descending magnitude;
Let $\lambda_{1,p}=[\mathbf{\Lambda}_1]_{z_p,z_p}$ denote the pth largest element, and $z_p\in\{1,2,\cdots,3K\}$, denote its corresponding position in the diagonal elements of $\mathbf{\Lambda}_1$, which is obtained during the sorting process;
The diagonal elements of $\tilde{\mathbf{\Lambda}}_2$ are rearranged following the order specified by the index arrayz_p, and the pth largest element in this sorted sequence is denoted by $\lambda_{2,p}=\left[\tilde{\mathbf{\Lambda}}_2\right]_{z_p,z_p}$;

The eigenvalue decomposition of these matrices is given by:

$$\mathbf{F}_x=\mathbf{E}_x\mathbf{\Lambda}_x\mathbf{E}_x^{\mathrm{H}},\mathbf{F}_y=\mathbf{E}_y\mathbf{\Lambda}_y\mathbf{E}_y^{\mathrm{H}} \tag{52}$$

$$\mathbf{E}_x=\begin{bmatrix}\mathbf{E}_{x11} & \mathbf{E}_{x12}\\ \mathbf{E}_{x21} & \mathbf{E}_{x22}\end{bmatrix},\mathbf{E}_y=\begin{bmatrix}\mathbf{E}_{y11} & \mathbf{E}_{y12}\\ \mathbf{E}_{y21} & \mathbf{E}_{y22}\end{bmatrix} \tag{53}$$

Let $\mathbf{E}_x\in\mathbb{C}^{6K\times6K}$ and $\mathbf{E}_y\in\mathbb{C}^{6K\times6K}$ denote the eigenvector matrices corresponding to $\mathbf{F}_x$ and $\mathbf{F}_y$, respectively. The diagonal matrices $\mathbf{\Lambda}_x\in\mathbb{C}^{6K\times6K}$ and $\mathbf{\Lambda}_y\in\mathbb{C}^{6K\times6K}$ contain the associated eigenvalues along their main diagonals. To summarize, the final estimates of $\mathbf{\Psi}_1$ and $\mathbf{\Psi}_2$ are derived as follows:

$$\hat{\mathbf{\Psi}}_1=-\mathbf{E}_{x12}\mathbf{E}_{x22}^{-1},\ \hat{\mathbf{\Psi}}_2=-\mathbf{E}_{y12}\mathbf{E}_{y22}^{-1} \tag{54}$$

It is feasible to use the eigenvalues of $\hat{\mathbf{\Psi}}_1$ and $\hat{\mathbf{\Psi}}_2$ as estimates of the diagonal elements of $\mathbf{\Phi}_1$ and $\mathbf{\Phi}_2$, respectively. Due to possible eigenvalue ordering discrepancies, direct pairing may result in mismatches. Fortunately, based on the relationships among $\tilde{\mathbf{Q}}\mathbf{B}$, $\mathbf{\Omega}\mathbf{B}$, $\mathbf{J}_3\mathbf{B}$ and $\mathbf{J}_4\mathbf{B}$, it can be shown that $\mathbf{\Psi}_1$ and $\mathbf{\Psi}_2$ have the same eigenvector matrix. This property enables eigenvalue pairing of $\hat{\mathbf{\Psi}}_1$ and $\hat{\mathbf{\Psi}}_2$ by applying a matching technique [17], as described in Algorithm 1.

Assuming that $\xi_{1,q}$ and $\xi_{2,q}$ represent the eigenvalues of the qth pair of matches, $k=1,2,\cdots,K$. In summary, the parameters of the kth ID source are computed as follows:

$$\xi_{1,3(k-1)+r}\approx\exp\left(ju\sin(\phi_k)\cos(\theta_k)\right) \tag{55}$$

$$\xi_{2,3(k-1)+r}\approx\exp\left(ju\sin(\phi_k)\sin(\theta_k)\right) \tag{56}$$

$$\hat{\theta}_k=\frac{1}{3}\sum_{r=1}^{3}\tan^{-1}\left(\frac{\ln(\xi_{2,3(k-1)+r})}{\ln(\xi_{1,3(k-1)+r})}\right) \tag{57}$$

$$\hat{\phi}_k=\frac{1}{3}\sum_{r=1}^{3}\sin^{-1}\left(\frac{1}{u}\sqrt{-\sum_{p=1}^{2}\left(\ln(\xi_{p,3(k-1)+r})\right)^2}\right) \tag{58}$$

Given that each eigenvalue of $\mathbf{\Psi}_1$ and $\mathbf{\Psi}_2$ is repeated three times, the repeated values are averaged to obtain the nominal DOA estimates in both azimuth and elevation.

Based on the beamspace reception measurements, an estimate of $\mathbf{\Lambda}_v$ can be obtained, and the noise covariance is estimated by averaging the PM_y-3K smallest eigenvalues of $\mathbf{R}_y$.

$$\hat{\mathbf{\Lambda}}_v=\hat{\mathbf{B}}^{\dagger}(\mathbf{R}_y-\hat{\sigma}_n^2\mathbf{I}_{PM_y})(\hat{\mathbf{B}}^{\mathrm{H}})^{\dagger}\in\mathbb{C}^{3K\times3K} \tag{59}$$

The angle spread based on $\mathbf{\Lambda}_v$ is computed as follows:

$$\hat{\sigma}_{\theta_k}=\sqrt{\frac{[\hat{\mathbf{\Lambda}}_v]_{K+k,K+k}}{[\hat{\mathbf{\Lambda}}_v]_{k,k}}},k=1,2,\ldots,K \tag{60}$$

$$\hat{\sigma}_{\phi_k}=\sqrt{\frac{[\hat{\mathbf{\Lambda}}_v]_{2K+k,2K+k}}{[\hat{\mathbf{\Lambda}}_v]_{k,k}}},k=1,2,\ldots,K \tag{61}$$

2) Measurement noise computation: In the DOA tracking problem of massive MIMO systems, the measurement errors mainly stem from two aspects. The physical noise introduced by the sensor or system hardware, and the estimator errors generated by the signal processing algorithm itself. In the DOA estimation scenario of ID signal source, the real measurement error cannot be obtained directly, and the empirical error depends heavily on the implementation details of the specific estimation algorithm (such as subspace estimation method, snapshot number, noise subspace dimension estimation error, etc.), which is difficult to be used as a stable and interpretable noise model input. Under the conditions of high SNR and large samples, CRB can accurately approximate the actual estimation error, and the verification estimator is the main factor determining the measurement uncertainty. After array processing and signal fusion, the residual physical noise becomes relatively insignificant, and the statistical characteristics of the measurement error are mainly determined by the performance of the estimator.

Therefore, the measurement error in the ID sources tracking process primarily arises from the DOA estimation. The CRB of the estimated angular parameters is employed as a substitute for the noise covariance in the tracking process. The process begins with approximating the AM matrix, followed by the computation of the corresponding covariance matrix. Subsequently, CRB is derived based on the Fisher information matrix (FIM).

$$\begin{aligned}&\left[\mathbf{a}\left(\theta_{k,j}(t),\phi_{k,j}(t)\right)\right]_m \approx \mathbf{a}_1\left(\theta_{k,j}(t),\phi_{k,j}(t)\right)\\ &\times\mathbf{a}_2\left(\theta_{k,j}(t),\phi_{k,j}(t)\right)\times\mathbf{a}_3\left(\theta_{k,j}(t),\phi_{k,j}(t)\right)\end{aligned} \tag{62}$$

$$\begin{aligned}&\mathbf{a}_1\left(\theta_{k,j}(t),\phi_{k,j}(t)\right)=\exp(iu\sin(\bar{\phi}_k)\times\\ &\left[(m_{\mathrm{x}}-1)\cos(\bar{\theta}_k)+(m_{\mathrm{y}}-1)\sin(\bar{\theta}_k)\right]^{\mathrm{T}}\end{aligned} \tag{63}$$

$$\begin{aligned}&\mathbf{a}_2\left(\theta_{k,j}(t),\phi_{k,j}(t)\right)=\exp\Big(iu\tilde{\phi}_{k,j}(t)\cos(\bar{\phi}_k)\times\\ &\left[(m_{\mathrm{x}}-1)\cos(\bar{\theta}_k)+(m_{\mathrm{y}}-1)\sin(\bar{\theta}_k)\right]\Big)\end{aligned} \tag{64}$$

$$\begin{aligned}&\mathbf{a}_3\left(\theta_{k,j}(t),\phi_{k,j}(t)\right)=\exp\Big(iu\tilde{\theta}_{k,j}(t)\times\sin(\bar{\phi}_k)\times\\ &\left[-(m_{\mathrm{x}}-1)\sin(\bar{\theta}_k)+(m_{\mathrm{y}}-1)\cos(\bar{\theta}_k)\right]\Big)\end{aligned} \tag{65}$$

Based on the prior approximation of the AM matrix, the corresponding covariance matrix is subsequently computed to support CRB derivation.

$$\mathbf{R}_{\mathbf{z}}\approx\sum_{k=1}^{K}\sigma_k^2\boldsymbol{\Xi}_k+\sigma_{\mathrm{n}}^2\mathbf{I}_M\in\mathbb{C}^{M\times M} \tag{66}$$

$$\boldsymbol{\Xi}_k=\left(\ \mathbf{a}(\bar{\theta}_k,\bar{\phi}_k)\mathbf{a}^{\mathrm{H}}(\bar{\theta}_k,\bar{\phi}_k)\ \right)\odot\mathbf{B}_k=\mathbf{D}_k\mathbf{B}_k\mathbf{D}_k^{\mathrm{H}} \tag{67}$$

$$\mathbf{D}_k=\mathrm{diag}(\mathbf{a}(\bar{\theta}_k,\bar{\phi}_k))\in{}^{M\times M} \tag{68}$$

$$\begin{aligned}&[\mathbf{B}_k]_{m,n}=\exp\Big(-(\sigma_{\phi_k}^2\cos^2(\bar{\phi}_k)\times\\ &[\delta_{\mathrm{x}}\cos(\bar{\theta}_k)+\delta_{\mathrm{y}}\sin(\bar{\theta}_k)]^2+\sigma_{\theta_k}^2\sin^2(\bar{\phi}_k)\times\\ &\left[-\delta_{\mathrm{x}}\sin(\bar{\theta}_k)+\delta_{\mathrm{y}}\cos(\bar{\theta}_k)\right]^2)\times u^2/2\Big)\end{aligned} \tag{69}$$

The critical step is the accurate formulation of the FIM. In this work, following the methodology presented in [17], the received measurements and noise are partitioned into block matrices, denoted as $\mathbf{v}=\left[\sigma_1^2,\cdots,\sigma_K^2,\sigma_n^2\right]^{\mathrm{T}}$, $\mathbf{u}=[\mathbf{u}_{\bar{\theta}}^{\mathrm{T}},\mathbf{u}_{\bar{\phi}}^{\mathrm{T}},\mathbf{u}_{\sigma_\theta}^{\mathrm{T}},\mathbf{u}_{\sigma_\phi}^{\mathrm{T}}]^{\mathrm{T}}$ and $\xi=[\mathbf{u}^{\mathrm{T}},\mathbf{v}^{\mathrm{T}}]^{\mathrm{T}}$, where the specific parameters involved include $\mathbf{u}_{\bar{\theta}}=[\bar{\theta}_1,\bar{\theta}_2,\cdots,\bar{\theta}_K]^{\mathrm{T}}$ and $\mathbf{u}_{\sigma_\theta}=[\sigma_{\theta_1},\sigma_{\theta_2},\cdots,\sigma_{\theta_K}]^{\mathrm{T}}$, the corresponding parameters for elevation follow a similar structure.

Then the FIM is calculated as follows.

$$[\mathbf{J}_{\xi,\xi}]_{q,q'}=T\mathrm{tr}\left(\mathbf{R}_{\mathbf{z}}^{-1}\frac{\partial\mathbf{R}_{\mathbf{z}}}{\partial[\xi]_q}\mathbf{R}_{\mathbf{z}}^{-1}\frac{\partial\mathbf{R}_{\mathbf{z}}}{\partial[\xi]_{q'}}\right) \tag{70}$$

where, $q=q'=1,2,\cdots,5K+1$, T denotes the number of snapshots of the received measurements. The FIM is partitioned into block matrices based on the structure of the received measurements and noise components. To derive the CRB for the covariance of the angular parameter estimates, the block matrix inversion theorem is employed.

$$\mathbf{J}_{\xi,\xi}=\begin{bmatrix}\mathbf{J}_{\mathbf{u},\mathbf{u}} & \mathbf{J}_{\mathbf{u},\mathbf{v}}\\ \mathbf{J}_{\mathbf{u},\mathbf{v}}^{\mathrm{T}} & \mathbf{J}_{\mathbf{v},\mathbf{v}}\end{bmatrix} \tag{71}$$

$$\mathrm{E}\left\{(\hat{\mathbf{u}}-\mathbf{u})(\hat{\mathbf{u}}-\mathbf{u})^{\mathrm{T}}\right\}\geq\left(\mathbf{J}_{\mathbf{u},\mathbf{u}}-\mathbf{J}_{\mathbf{u},\mathbf{v}}\mathbf{J}_{\mathbf{v},\mathbf{v}}^{-1}\mathbf{J}_{\mathbf{u},\mathbf{v}}^{\mathbf{T}}\right)^{-1} \tag{72}$$

A detailed summary of the measurement generation process is presented in Algorithm 2. The measurement model mainly consists of two parts: One part is using the UESPRIT algorithm to extract pseudo-measurements of the signal sources at each moment, which reflect the instantaneous results of the signal sources; the other part is to more accurately represent the characteristics of measurement errors, we introduce the CRB into the model, thereby providing a theoretically achievable noise constraint for the subsequent filtering stages. Through this design, the measurement model not only reflects the time-varying characteristics of the signal sources, but also fully accounts for estimation uncertainty, laying a reliable foundation for multi-source joint state estimation.

Algorithm 2 Measurement Generation Algorithm.

Converting element-space measurements to beamspace measurements: $\mathbf{z}_i(t)=\mathbf{W}^{\mathrm{H}}\mathbf{y}_i(t)=\mathbf{B}_i\mathbf{v}(t)+\mathbf{W}^{\mathrm{H}}\mathbf{n}_i(t)$
Computing the covariance matrix and performing EVD: $\mathbf{R}_z=\mathrm{E}\left\{\mathbf{z}(t)\mathbf{z}^{\mathrm{T}}(t)\right\}=\mathbf{U}_s\boldsymbol{\Sigma}_s\mathbf{U}_s^{\mathrm{H}}+\sigma_n^2\mathbf{U}_n\mathbf{U}_n^{\mathrm{H}}$
Determine the rotational invariance relation:
$\tilde{\mathbf{Q}}\mathbf{U}_s=\Omega\mathbf{U}_s\mathbf{T}\boldsymbol{\Phi}_1\mathbf{T}^{-1}=\Omega\mathbf{U}_s\boldsymbol{\Psi}_1$;
$\mathbf{J}_4\mathbf{U}_s=\mathbf{J}_3\mathbf{U}_s\mathbf{T}\boldsymbol{\Phi}_2\mathbf{T}^{-1}=\mathbf{J}_3\mathbf{U}_s\boldsymbol{\Psi}_2$;
The paired nominal angles are estimated using the least squares method as formulated in equations (57)–(58);
The angular spreads are estimated using the formulations provided in equations (60)–(61);
Calculate the multi-signal source CRB;
Generated ID source measurement:
$Z_k=\mathbf{Z}_k+\mathbf{w}_k,\mathbf{w}_k\sim\mathcal{N}(\mathbf{0},\mathbf{R}_k)$
$\mathbf{R}_k\approx CRB(\mathbf{Z}_k)$

3) Update the state: Since the GLMB filter for ID signal sources follows a conjugate prior distribution, its posterior distribution is identical to the multi ID signal sources prediction form, expressed as follows:

$$\begin{aligned}\pi_+(X)=\Delta(X)&\sum_{(I_+,\xi)\in\mathcal{F}(\mathbb{L}_+)\times\Xi,\theta\in\Theta}w_+^{(I,\xi,\varepsilon)}(Z)\\ &\delta_I[\mathcal{L}(X)][p(\cdot;\xi,\varepsilon(l))]^X\end{aligned} \tag{73}$$

$$w_{+}^{(I,\xi,\varepsilon)}(Z) \propto \left[\mu_Z(\cdot;\xi,\varepsilon(l))\right]^I w^{(I,\xi)} \tag{74}$$

$$\mu_Z(\cdot;\xi,\varepsilon(l)) = \sum\nolimits_{n=1}^{J^{(\xi)}(l)} w_n^{(\xi)}(l_i)\,\psi_Z\left(\mathbf{x}_{\mathbf{n}}^{(\xi)}(\mathbf{l}),\mathbf{l};\varepsilon\right) \tag{75}$$

$$p_Z(\cdot;\xi,\varepsilon(l)) = \left\{\left(\frac{\psi_Z(\cdot,l;\varepsilon(l))\,w_n^{(\xi)}(l)}{\mu_Z(\cdot;\xi,\varepsilon(l))},\mathbf{x}_{\mathbf{n}}^{(\xi)}(\mathbf{l})\right)\right\}_{n=1}^{J^{(\xi)}(l)} \tag{76}$$

$$\psi_Z(\cdot,l;\varepsilon(l)) = \begin{cases} p_D(\mathbf{x},\mathbf{l})\,g\left(z_{\varepsilon(l)}|\mathbf{x},\mathbf{l}\right), \varepsilon(l) > 0 \\ 1 - p_D(\mathbf{x},\mathbf{l}), \varepsilon(l) = 0 \end{cases} \tag{77}$$

The above equation details the calculation process for updating weights and probability distributions across multiple ID signal sources. Σ represents the measurement correlation mapping, where $\varepsilon :\to \{0,1,\cdots,|Z|\}$ and $\varepsilon(i) = \varepsilon(j) > 0 \Rightarrow i = j$, $g\left(z_{\varepsilon(l)}|\mathbf{x},\mathbf{l}\right)$ denote the measurement likelihood functions, and $p_D(\mathbf{x},\mathbf{l})$ signifies the detection probability.

IV. GLMB Smoother for Incoherently Distributed Sources

Compared to unidirectional filtering, the GLMB smoother generates more continuous, complete, and stable multi-target trajectories. It avoids trajectory discontinuities or fragmentation caused by transient outliers and maintains high robustness even in high-noise or weak-signal environments. Simultaneously, the GLMB smoother preserves label consistency during backward smoothing, ensuring long-term target trajectory identifiability. Therefore, this paper further employs the GLMB smoother in place of a filter to address the ID signal source tracking problem in massive MIMO environments. First, the forward GLMB filtering step is executed. Subsequently, at each time step, the most probable hypothesis with the highest marginal probability in the GLMB density is updated, transmitting the estimated trajectory information to the estimator for trajectory pruning. Finally, RTS smoothing techniques are applied to each trajectory to generate the smoothed state estimates.

A. Joint prediction and update

To prevent the propagation of predicted components that contribute insignificantly to the update process and to reduce the computational burden caused by excessive truncation operations, joint prediction and update strategy [37] is employed. This approach enables the direct recursion of two GLMB densities across consecutive time steps. Given the GLMB prior density and observation model, posterior density can be expressed as:

$$\begin{aligned}\pi_{Z_+}(X) \propto{}& \Delta(X) \sum_{I,\xi,I_+,\varepsilon_+} \omega^{(I,\xi)}\omega_{Z_+}^{(I,\xi,I_+,\varepsilon_+)} \\ &\times\delta_{I_+}(\mathcal{L}(X)[p_{Z_+}^{(\xi,\varepsilon_+)}]^X\end{aligned} \tag{78}$$

where, I denotes the set of ID signal sources labels, and $\xi \in \Xi$ represents the history of association maps. ξ captures the history of measurement-to-track associations. The specific parameters involved are computed as shown below.

$$\begin{aligned}\omega_{Z_+}^{(I,\xi,I_+,\varepsilon_+)} &= 1_{\Sigma_+(I_+)}(\varepsilon_+)[1-\bar{P}_S^{(\xi)}]^{I-I_+}[\bar{P}_S^{(\xi)}]^{I\cap I_+} \\ &\times[1-r_{B+}]^{+-I_+}[r_{B+}]^{+\cap I_+}[\bar{\psi}_{Z_+}^{(\xi,\varepsilon_+)}]^{I_+}\end{aligned} \tag{79}$$

$$P_S^{(\xi)}(l) = \left\langle p^{(\xi)}(\cdot,l), p_S(\cdot,l)\right\rangle \tag{80}$$

$$\bar{\psi}_{Z_+}^{(\xi,\varepsilon_+)}(l_+) = \left\langle p_+^{(\xi)}(\cdot,l_+), \psi_{Z_+}^{(\varepsilon_+(l_+))}(\cdot,l_+)\right\rangle \tag{81}$$

$$p_{Z_+}^{(\xi,\varepsilon_+)}(\mathbf{x}_+,l_+) = \frac{\bar{p}_+^{(\xi)}(x_+,l_+)\psi_{Z_+}^{(\varepsilon_+(l_+))}(\mathbf{x}_+,l_+)}{\bar{\psi}_{Z_+}^{(\xi,\varepsilon_+)}(l_+)} \tag{82}$$

$$\begin{aligned}\bar{p}_+^{(\xi)}(\mathbf{x}_+,l_+) &= 1_{\mathrm{L}}(\{l_+\})\frac{\left\langle p_S(\cdot,l_+)f_{S+}(\mathbf{x}_+|\cdot,l_+),p^{(\xi)}(\cdot,l_+)\right\rangle}{\bar{P}_S^{(\xi)}(l_+)} \\ &+1_{\mathrm{B}_+}(\{l_+\})p_{B+}(\mathbf{x}_+,l_+)\end{aligned} \tag{83}$$

The details of the GLMB Smoother for ID signal sources iterative estimation process is given in Algorithm 3.

B. Trajectory estimation

The GLMB filter provides a maximum a posteriori estimate of the ID source state at the end of each filtering cycle, with the state mean evaluated based on the estimated cardinality. In the GLMB smoother, the cardinality and state estimation hypotheses for $\{(I,\zeta)_h\}_{h=1:H}$ are computed as follows:

$$\hat{N} = \arg\max(\rho) = \arg\max\left(\sum_{\xi\in\left\{(I,\zeta)_h\right\}_{h=1:H}} w^{\xi}\delta_n\left(\left|I^{(\xi)}\right|\right)\right) \tag{84}$$

$$\hat{\xi} = \arg\max_{(\xi)} w^{\xi}\delta_{\hat{N}}\left(\left|I^{(\xi)}\right|\right) \tag{85}$$

Next, the estimated trajectories at the current time step t are denoted as $\hat{\zeta}_t = \left\{\left(\hat{l}_1^t,\hat{b}_{\hat{l}_{1_1}^t},\hat{\varsigma}_{\hat{l}_1^t}\right),\cdots,\left(\hat{l}_{\hat{N}}^t,\hat{b}_{\hat{l}_{\hat{N}}^t},\hat{\varsigma}_{\hat{l}_{\hat{n}}^t}\right)\right\}$, and the set of all estimated trajectories from the initial time step to the t is expressed as $\hat{\zeta} = \left\{\left(\hat{l}_1,\hat{b}_{\hat{l}_1},\hat{\varsigma}_{\hat{l}_1}\right),\cdots,\left(\hat{l}_N,\hat{b}_{\hat{l}_N},\hat{\varsigma}_{\hat{l}_N}\right)\right\}$. And at the end of each filtering step, the association history of each existing trajectory, as well as their corresponding initial birth states, are updated accordingly. Subsequently, the RTS smoothing technique is applied to each trajectory to obtain the corresponding smoothed state estimates. Here, $\hat{l}_{\hat{n}}^t$ is the labeling of the estimated trajectory n at time t, $\hat{b}_{\hat{l}_{\hat{n}}^t}$ represents its corresponding initial birth state, and $\hat{\varsigma}_{\hat{l}_{\hat{n}}^t}$ is the corresponding association history.

C. Single ID signal source RTS smoother

The GLMB smoother improves the estimation accuracy of the GLMB filter by incorporating a backward RTS smoothing step. This enhancement facilitates the suppression of anomalies in the filtered results and the elimination of trajectory fragmentation, resulting in more continuous and accurate smoothed trajectories. Following the forward GLMB filtering stage, the final-time filtering estimate is utilized to initialize the backward RTS smoothing step. The complete smoothing procedure is outlined as follows:

$$\bar{\mathbf{x}}_{t+1} = F\mathbf{x_t} \tag{86}$$

$$\bar{P}_{t+1} = FP_tF^{\mathrm{T}} + Q \tag{87}$$

$$D = P_{t+1}F(\bar{P}_{t+1})^{-1} \tag{88}$$

$$P_t^s = P_t + D(P_{t+1}^s - \bar{P}_{t+1})D^{\mathrm{T}} \tag{89}$$

here, $\mathbf{x}$ represents the ID source state, F is the transformation matrix, Q denotes the process noise, and the superscript s corresponds to the smoothed estimate.

V. Algorithm Complexity Analysis

The overall computational complexity of the proposed algorithm primarily concentrates on three components:

1) Pseudo-measurement generation (based on UESPRIT), the complexity of the proposed algorithm in case $M \to \infty$ is primarily determined by the following steps. The complexity of applying the beamspace transformation to obtain the beamspace observations and covariance matrix, as well as performing EVD, is on the order of $\mathcal{O}(PM_yN) + \mathcal{O}\left((PM_z)^3 + (PM_z)^2N\right)$. And the complexity of determining matched DOAs based on rotational invariance relationships is $\mathcal{O}\left(PM_zK^2\right)$. Due to $M \to \infty$, the complexity of this part approaches $\mathcal{O}\left((PM_z)^3\right)$. Although the overall algorithm exhibits high computational complexity, its performance improvements in estimation accuracy, signal source discrimination, and trajectory continuity effectively compensate for the increased computational burden.

2) GLMB filter part, the complexity of the prediction and update step mainly from the number of assumptions, while the complexities of the remaining steps are relatively low and can be omitted. The complexity is $\mathcal{O}_{pre}\left(N_{h,k-1} \times N_{surv} \times N_{birth}\right)$. They represent the number of hypothetical sources at the previous moment, as well as the number of surviving ID sources and newly emerged ID sources at the current moment. The data association in update assumes weighted hypotheses and label recursion, with a complexity of $\mathcal{O}_{up}\left(N_{h,k-1} \times H_k\right)$, representing the number of ID sources and the number of hypotheses, respectively.

3) GLMB smoother part, the total computational complexity is the sum of the forward GLMB filtering complexity and the trajectory-based RTS smoothing complexity. Applying RTS smoothing to a trajectory of length T_i incurs a cost of $\mathcal{O}\left(\sum_{i=1}^{L} T_i\mathbf{x}^3\right)$, where $\mathbf{x}$ denotes the dimensionality of a single ID state, L is total number of trajectories.

Therefore, the complexity of the ID sources tracking method based on GLMB filter and GLMB smoother are represented as follows:

$$\mathcal{O}_{filter} = \mathcal{O}\left((PM_y)^3\right) + \mathcal{O}_{pre}\left(N_{h,k-1} \times N_{surv} \times N_{birth}\right) + \mathcal{O}_{up}\left(N_{h,k-1} \times H_k\right) \tag{90}$$

$$\mathcal{O}_{smoother} = \mathcal{O}_{filter} + \mathcal{O}\left(\sum_{i=1}^{L} T_i\mathbf{x}^3\right) \tag{91}$$

VI. Experimental Simulation Analysis

To evaluate the tracking accuracy achieved by the proposed algorithm, its tracking performance is analyzed in this section through simulations under two experimental scenarios. The experimental simulations are based on the URA configuration depicted in Fig. 1, with the massive MIMO system comprising $M = 100$ array elements. $SNR = 10\log(\sigma_i^2/\sigma_n^2)$. The

Algorithm 3 GLMB Smoother Iterative Estimation Algorithm.

for $n = 1 : N$
 Initialize the newborn signal source state:
 $\left\{\bar{m}^{l_n}_{t_i^{\hat{l}_n}}, \bar{P}^{l_n}_{t_i^{\hat{l}_n}}\right\} \leftarrow \hat{b}_{\hat{l}_n}$
 Update surviving signal source state:
 $\left\{\tilde{m}^{l_n}_{t_i^{\hat{l}_n}}, \tilde{P}^{l_n}_{t_i^{\hat{l}_n}}\right\} \leftarrow \left(\bar{m}^{l_n}_{t_i^{\hat{l}_n}}, \bar{P}^{l_n}_{t_i^{\hat{l}_n}}, z^{t_i^{\hat{l}_n}}_{\hat{\zeta}^{t_i^{\hat{l}_n}}_{\hat{l}_n}}\right)$
 if $\hat{l}^t_n \in \{\hat{l}_1, ..., \hat{l}_N\}$
 replace the tuple $(\hat{l}^t_n, \hat{b}_{\hat{l}^t_n}, \hat{\zeta}_{\hat{l}^t_n})$ of trajectories labeled
 else
 adding a newborn target trajectory tuple $\hat{=}\hat{\cup}(\hat{l}^t_n, \hat{b}_{\hat{l}^t_n}, \hat{\zeta}_{\hat{l}^t_n})$
 end
 for $t = t_i^{\hat{l}_n} + 1 : t_e^{\hat{l}_n}$
 single-target projections $\left\{\bar{m}^{l_n}_t, \bar{P}^{l_n}_t\right\} \leftarrow \left(\tilde{m}^{l_n}_{t-1}, \tilde{P}^{l_n}_{t-1}\right)$
 if $\hat{\zeta}^t_{\hat{l}_n} = 0$
 $\left\{\tilde{m}^{l_n}_t, \tilde{P}^{l_n}_t\right\} = \left\{\bar{m}^{l_n}_t, \bar{P}^{l_n}_t\right\}$
 else
 single-target updates $\left\{\tilde{m}^{l_n}_t, \tilde{P}^{l_n}_t\right\} \leftarrow \left(\bar{m}^{l_n}_t, \bar{P}^{l_n}_t, z^t_{\hat{\zeta}^t_{\hat{l}_n}}\right)$
 end
 end
 Signal source backward smoothing:
 $\left\{m^{\hat{l}_n}_t, P^{\hat{l}_n}_t\right\}_{t_i^{\hat{l}_n}:t_e^{\hat{l}_n}} \leftarrow \left(\left\{\tilde{m}^{\hat{l}_n}_t, \tilde{P}^{\hat{l}_n}_t\right\}_{t_i^{\hat{l}_n}:t_e^{\hat{l}_n}}\right)$
 filtering result from the final time step is utilized as the initial condition for the backward smoothing operation
 for $t = N-1 : -1 : 1$
 Implementation of formulas (86)-(89);
 end
end

evaluation is based on the generalized optimal sub-pattern assignment (GOSPA) distance [38], configured with $\alpha = 2$, $p = 2$, and $c = 3$, to quantify both localization and cardinality errors. In the following experimental simulations, set $p_{S,t} = 0.99$, $p_{D,t} = 0.99$. The effectiveness of the proposed tracking approach is demonstrated by comparing its performance against the Beamspace-UESPRIT-GLMB Filter, the ESPRIT-GLMB Smoother, and the ESPRIT-GLMB Filter. All algorithms are evaluated over 500 Monte Carlo (MC) simulation runs to ensure the reliability and statistical significance of the results.

A. Experiment I

In this experimental scenario, a CV motion model is established for four ID signal sources, with no crossover occurring during their propagation in the spatial domain. The angle spread of all ID signal sources is set to $\sigma_\theta = \sigma_\varphi = 1^\circ$.

$$F_t = \begin{bmatrix} 1 & \Delta T & 0 & 0 \\ 0 & 1 & 0 & 0 \\ 0 & 0 & 1 & \Delta T \\ 0 & 0 & 0 & 1 \end{bmatrix} \tag{92}$$

TABLE II
PARAMETERS OF THE NEWBORN SIGNAL SOURCES

Newborn ID signal sources	Survival probability	Sampling mean
ID signal source I	$\zeta_B^{(l,1)} = 0.02$	$m_1 = [20, 2, 90, -1]^{\mathrm{T}}$
ID signal source II	$\zeta_B^{(l,2)} = 0.03$	$m_2 = [160, -1, 70, -1]^{\mathrm{T}}$
ID signal source III	$\zeta_B^{(l,3)} = 0.03$	$m_3 = [80, 1.5, 5, 0.5]^{\mathrm{T}}$
ID signal source IV	$\zeta_B^{(l,4)} = 0.02$	$m_4 = [15, 3, 20, 1]^{\mathrm{T}}$

TABLE III
THE MOVEMENT STATUS AND SURVIVAL TIME OF THE SIGNAL SOURCES IN EACH TIME PERIOD

ID signal sources	Initial state	Survival time
ID signal source I	$\mathrm{x}_0^1 = [20, 2, 90, -1]^{\mathrm{T}}$	$1 - 30s$
ID signal source II	$\mathrm{x}_0^2 = [160, -1, 70, -1]^{\mathrm{T}}$	$10 - 35s$
ID signal source III	$\mathrm{x}_0^3 = [80, 1.5, 5, 0.5]^{\mathrm{T}}$	$10 - 40s$
ID signal source IV	$\mathrm{x}_0^4 = [15, 3, 20, 1]^{\mathrm{T}}$	$22 - 50s$

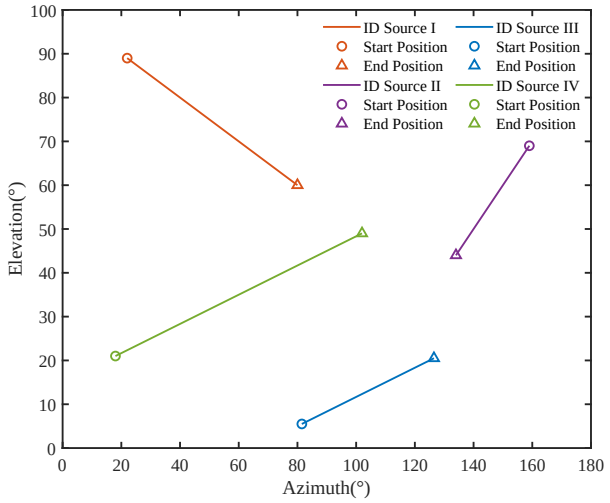

Fig. 2. True trajectory of the ID signal sources.

$$G_t = \begin{bmatrix} \Delta T^2/2 & 0 \\ \Delta T & 0 \\ 0 & \Delta T^2/2 \\ 0 & \Delta T \end{bmatrix} \tag{93}$$

where $Q = diag\left(\sigma_v^2 G_t\right)$, $\Delta T = 1s$ denotes the sampling time interval. For the experimental setup, $SNR = 20dB$ and the total data collection time is 50 seconds. The parameters of the newborn signal sources and the motion states of the signal sources at each time step are given in Tables II and III. The sampling covariance is set to $diag\{4, 1, 4, 1\}$.

The true trajectories of the ID signal sources moving in the spatial domain are shown in Fig. 2. The error comparison of the algorithm under different SNR conditions, as shown in the Fig. 3 compares the estimation errors of ID source tracking implemented with the GLMB filter, while Fig. 4 shows the comparison for ID source tracking based on the GLMB smoother. The figures demonstrate that the proposed algorithm exhibits larger tracking errors under low SNR conditions, with the estimation errors decreasing as the SNR increases.

The estimated tracking trajectories are illustrated in Fig. 5. The experimental results indicate that all four compared algorithms are capable of tracking the dynamic parameters of the ID signal sources in real time. This can be mainly attributed to the adaptability of the GLMB filter and smoother in tracking both the varying number and dynamic states of ID signal sources.

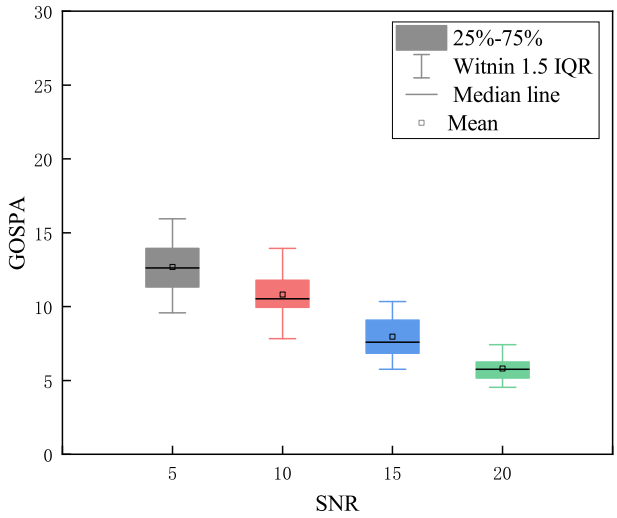

Fig. 3. UESPRIT-GLMB-Filter: Estimation Error under Different SNR.

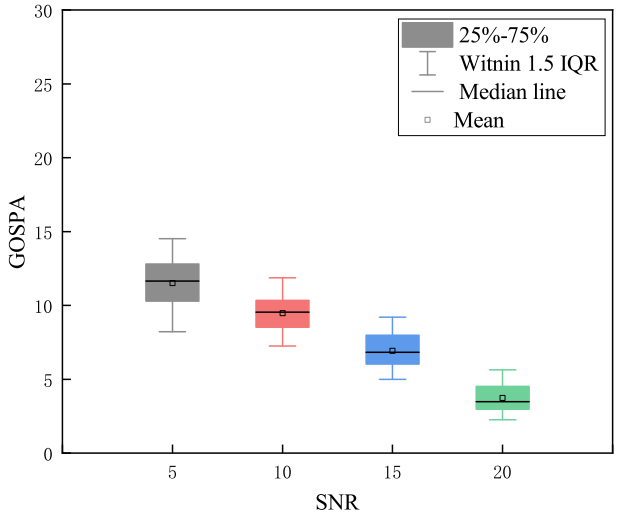

Fig. 4. UESPRIT-GLMB-Smoother: Estimation Error under Different SNR.

Fig. 6 presents the average number of ID sources estimated at each time step during the tracking process, and the shaded area indicates the deviation of the estimated values relative to the truth values across the MC simulations. It is evident from the simulation results that all four algorithms demonstrate a reasonable accuracy in estimating the number of sources and can generally reflect the trend of actual sources count over time. However, the ESPRIT-GLMB filter and ESPRIT-GLMB smoother exhibit higher estimation uncertainty compared to the Beamspace-based counterparts.

Fig. 7 to Fig. 9 present the local zoom-in views of the ID signal sources during the tracking process, and the rectangular

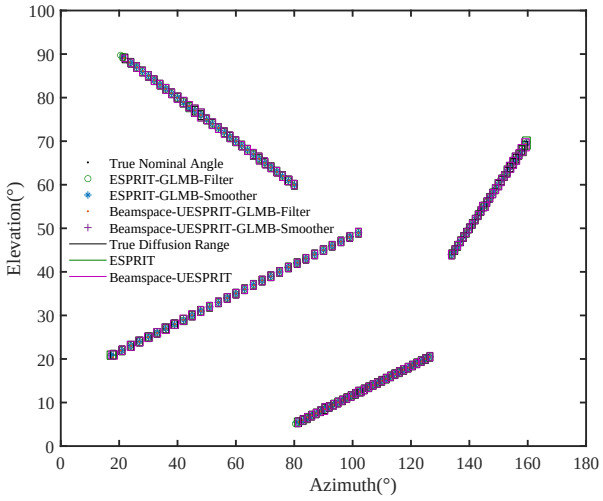

Fig. 5. ID signal source tracking trajectory.

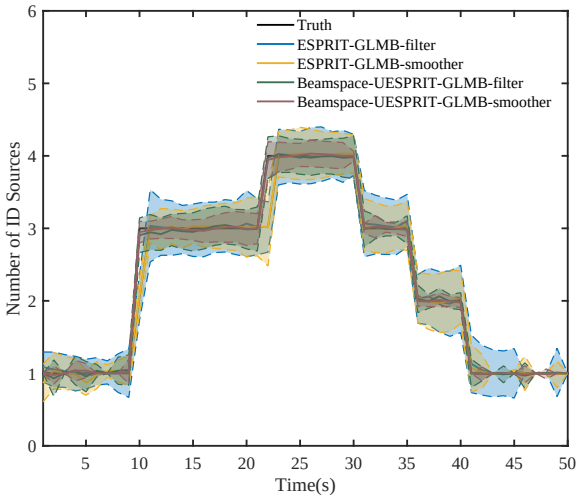

Fig. 6. Estimation of the number of ID signal sources.

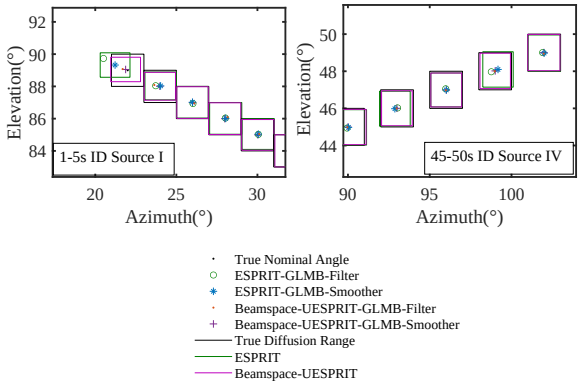

Fig. 7. 1-5s, 45-50s ID source tracking trajectory.

regions characterizes the dispersion property of the ID signal source in the spatial domain, i.e., the magnitude of the expansion angle.

Fig. 7 shows a local zoomed-in view of the tracking trajectories of the ID signal sources at both the initial and final stages within the 50-second observation period. It can be observed that all four algorithms exhibit rapid convergence during the initial stage and achieve relatively high estimation accuracy. In particular, the algorithms proposed in this paper provide nominal angle estimates at the appear and disappear moments that are closer to the true values, whereas the ESPRIT-GLMB filter and ESPRIT-GLMB smoother exhibit a certain degree of bias during these stages. Moreover, the smoother integrates state information from all the steps in the history, which significantly enhances estimation accuracy in dynamic scenarios. Compared to the ESPRIT algorithm, the Beamspace-UESPRIT algorithm provides a more accurate estimation of the ID signal sources. This improvement is primarily attributed to the beamspace concentrates the energy of the ID signal sources, thereby making them more distinguishable within the beamspace domain.

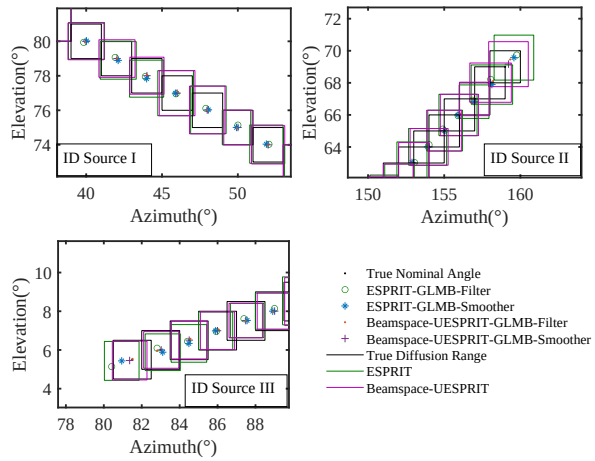

Fig. 8. 10-15s ID source tracking trajectory.

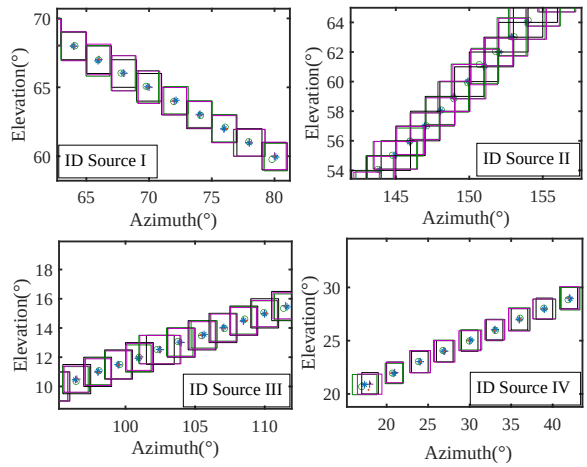

Fig. 9. 22-30s ID source tracking trajectory.

As shown in Figs. 8 and 9, which depict the tracking trajectories during time steps with an increasing number of

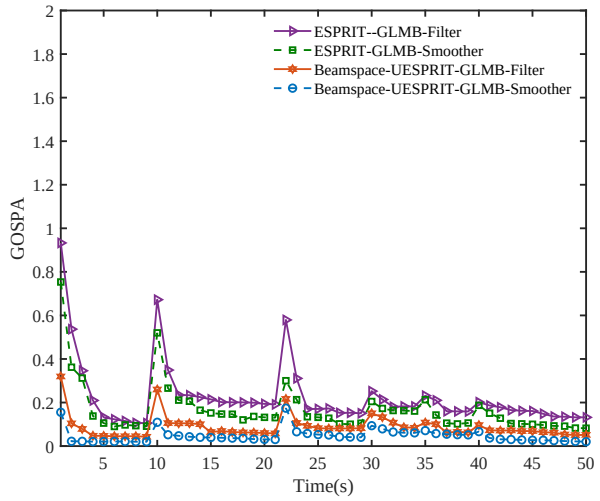

Fig. 10. ID signal source nominal angle error.

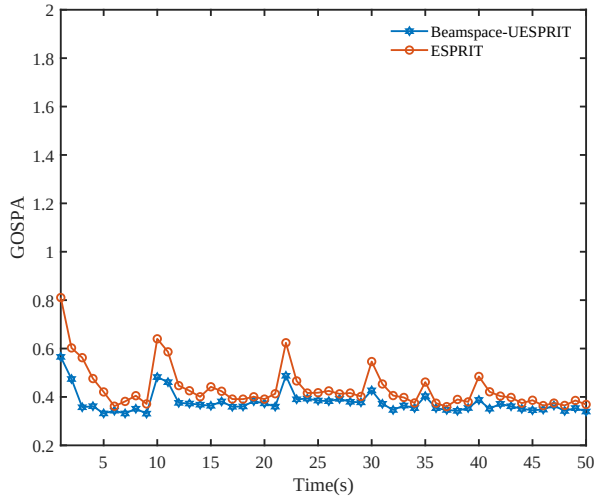

Fig. 11. ID signal source angle spread error.

ID sources, the proposed algorithm effectively detects newborn sources and yields more accurate estimates than the other three methods. In addition, the proposed method maintains superior tracking performance even for rapidly moving ID sources (e.g., ID source IV).

In contrast, the remaining algorithms exhibit larger estimation errors, which are clearly reflected in the tracking error curves shown in Fig. 10. Further analysis of the figures reveals that the smoother outperforms the filter in terms of overall estimation accuracy. Additionally, the Beamspace-UESPRIT algorithm demonstrates superior performance in estimating the parameters of the ID signal sources compared to the conventional ESPRIT algorithm. Although all four algorithms exhibit an increase in estimation error when the number of ID signal sources changes, the tracking performance gradually recovers over time, resulting in a reduction in estimation error. Notably, the algorithm proposed in this paper maintains a relatively low tracking error throughout the tracking process. Fig. 11 presents the tracking error of the angle spread of the ID

TABLE IV
PARAMETERS OF THE NEWBORN SIGNAL SOURCES

Newborn ID signal sources	Survival probability	Sampling mean
ID signal source I	$\zeta_B^{(l,1)} = 0.03$	$m_1 = [10, 3, 5, 1.5]^{\mathrm{T}}$
ID signal source II	$\zeta_B^{(l,2)} = 0.03$	$m_2 = [130, -2.5, 90, -1.5]^{\mathrm{T}}$
ID signal source III	$\zeta_B^{(l,3)} = 0.02$	$m_3 = [80, 2.3, 5, 1.3]^{\mathrm{T}}$
ID signal source IV	$\zeta_B^{(l,4)} = 0.02$	$m_4 = [15, 4, 90, -2.0]^{\mathrm{T}}$

TABLE V
THE MOVEMENT STATUS AND SURVIVAL TIME OF THE SIGNAL SOURCES IN EACH TIME PERIOD

ID signal sources	Initial state	Survival time
ID signal source I	$\mathrm{x}_0^1 = [210, 3, 5, 1.5]^{\mathrm{T}}$	$1 - 50s$
ID signal source II	$\mathrm{x}_0^2 = [130, -2.5, 90, -1.5]^{\mathrm{T}}$	$10 - 50s$
ID signal source III	$\mathrm{x}_0^3 = [80, 2.3, 5, 1.3]^{\mathrm{T}}$	$10 - 40s$
ID signal source IV	$\mathrm{x}_0^4 = [15, 4, 90, -2.0]^{\mathrm{T}}$	$20 - 50s$

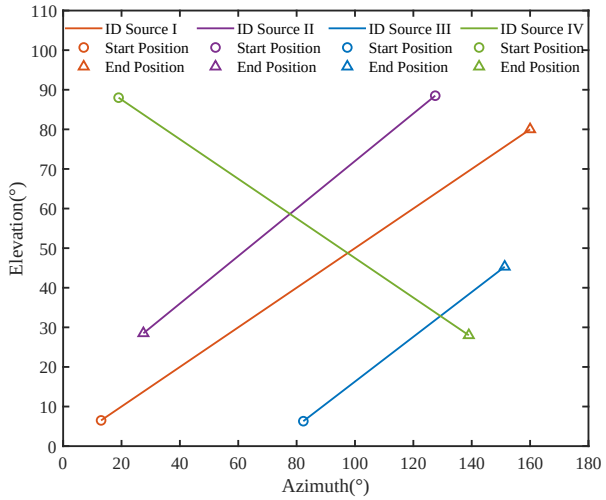

Fig. 12. True trajectory of the ID signal source.

signal sources, from which it is obvious that the Beamspace-UESPRIT algorithm has a better estimation performance with a relatively small estimation error.

B. Experiment II

A CV motion scenario is also configured for the ID signal sources; however, in this case, a transmission crossover occurs during the spatial propagation. The parameters of the newborn ID signal sources, as well as the motion states of the ID signal sources across different time intervals, are provided in Table IV and V. The sampling covariance is set to $diag\{10, 1, 10, 1\}$. All other simulation settings remain consistent with those used in Experiment I.

The true trajectory of the ID signal sources motion is shown in Fig. 12, while the estimated tracking trajectory is illustrated in Fig. 13. Fig. 14 presents the estimated average number of ID sources over time. It can be observed that all four algorithms are capable of timely identifying the appear and disappear of ID sources and estimating their number at each tracking time step. However, the ESPRIT-GLMB Filter and ESPRIT-GLMB Smoother exhibit greater estimation uncertainty. Fig.

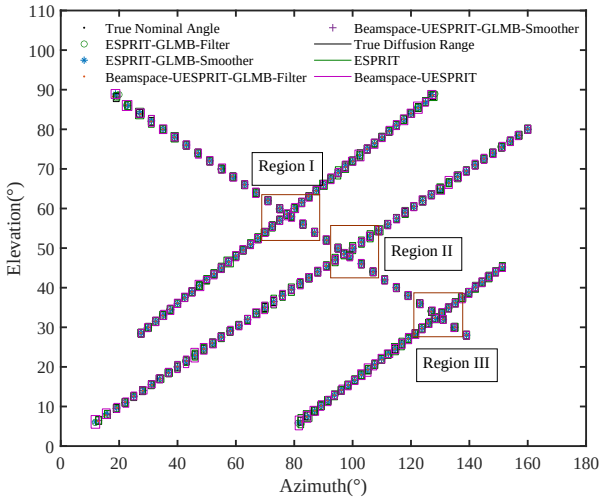

Fig. 13. ID signal sources tracking trajectory.

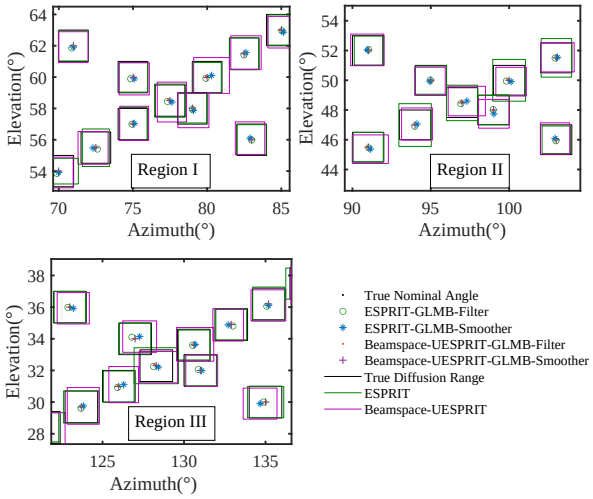

Fig. 15. Localized zoomed-in view of ID signal source.

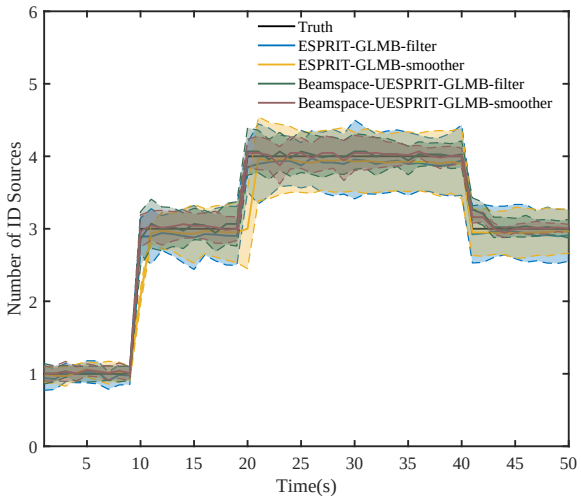

Fig. 14. Estimation of the number of ID signal sources.

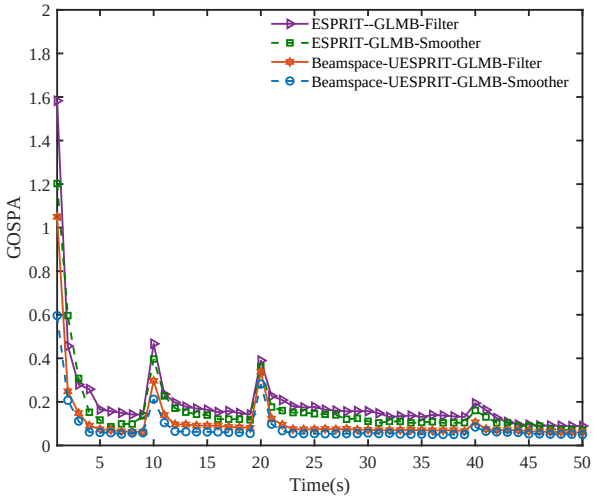

Fig. 16. ID signal source nominal angle error.

15 shows a zoomed-in view of three representative regions where crossover phenomena occur during tracking. The simulation results demonstrate that the Beamspace-UESPRIT-GLMB Smoother algorithm provides more accurate and continuous trajectory estimates. In contrast, the ESPRIT algorithm shows a certain degree of bias relative to the Beamspace-UESPRIT algorithm.

Fig. 16 presents the corresponding tracking errors. The comparative analysis indicates that the proposed algorithm demonstrates superior overall tracking performance, especially in handling time steps where multiple ID signal sources undergo crossover in the spatial domain. Compared with the other three algorithms, it achieves smaller estimation errors and recovers tracking accuracy more rapidly in subsequent time steps. This improvement is primarily attributed to the GLMB smoother, which fully exploits historical state information of the ID sources, thereby enabling self-correction in state estimation and enhancing the robustness of the tracking process. Moreover, the smoother demonstrates improved stability

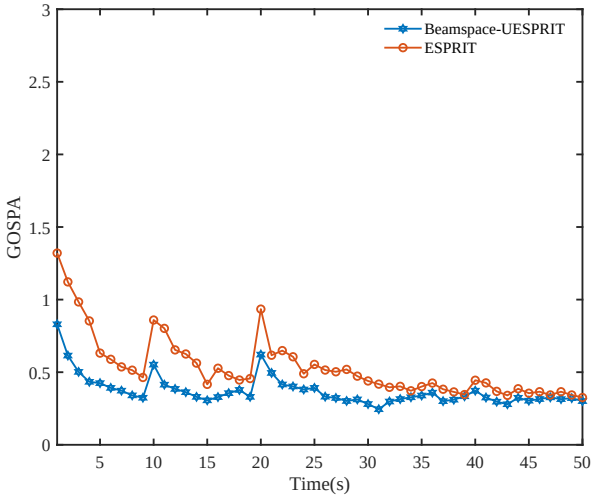

Fig. 17. ID signal source angle spread error.

in tracking ID sources by incorporating the time-dimensional information. The corresponding angle spread estimation errors, illustrated in Fig. 17, further substantiate the performance advantage in tracking ID sources.

VII. Conclusion

This study developed a novel tracking framework based on the GLMB filter and smoother to address the challenge of DOA estimation for dynamic ID sources in massive MIMO systems. The state sets and measurement sets of ID sources were effectively modeled using the RFS framework. At each time step, measurements were obtained through the beamspace UESPRIT algorithm, with the corresponding CRB for multiple ID sources utilized as the measurement noise covariance. The GLMB filter and smoother framework was then successfully applied to iteratively update the state estimates of ID sources over time. Simulation results demonstrated that the proposed Beamspace-UESPRIT-GLMB Smoother achieved accurate and real-time tracking of multiple ID sources, validating its effectiveness in practical scenarios. The key contributions of this work include: 1) the novel integration of beamspace processing with the GLMB framework; 2) the effective utilization of CRB as measurement noise covariance to enhance tracking precision. This research provides a robust solution for dynamic source tracking in complex electromagnetic environments, offering significant potential for applications in next-generation wireless communication systems. Future research directions may be pursued in the following areas. Real-time implementation of dynamic multi-source DOA tracking in large-scale array and high-speed scenarios continues to rely on techniques such as low-rank structure modelling, rapid matrix decomposition, and hardware acceleration to further enhance efficiency. Moreover, deep integration of DOA tracking with millimetre-wave radar, lidar, and visual sensors should be pursued for dense multi-source environments, thereby improving adaptive processing capabilities for complex target behaviours such as appearance, disappearance, and coalescence.

References

[1] Robin Chataut, Robert Akl, "Massive MIMO systems for 5G and beyond networks overview, recent trends, challenges, and future research direction," *Sensors.*, vol. 20, no. 10, pp. 2753, 2020.

[2] Y. Zhou, Z. Fei, S. Yang, J. Kuang, S. Chen and L. Hanzo, "Joint angle estimation and signal reconstruction for coherently distributed sources in massive MIMO systems based on 2-D unitary ESPRIT," *IEEE Access.*, vol. 5, pp. 9632-9646, 2017.

[3] A. Bose, A. Ghauri and M. Soltanalian, "Limits of transmit beamforming for massive MIMO radar," *in Proc. 54th Asilomar Conf. Signals, Syst., and Comput., CA, USA*, 2020, pp. 1157-1161.

[4] Y. Tian, W. Liu, H. Xu, S. Liu and Z. Dong,"2-D DOA estimation of incoherently distributed sources considering gain-phase perturbations in massive MIMO systems," *IEEE Trans. Wireless Commun.*, vol. 21, no. 2, pp. 1143-1155, Feb. 2022.

[5] S. Valaee, B. Champagne and P. Kabal,"Parametric localization of distributed sources," *IEEE Trans. Signal Process.*, vol. 43, no. 9, pp. 2144-2153, 1995.

[6] B. Tau Sieskul, "An asymptotic maximum likelihood for joint estimation of nominal angles and angular spreads of multiple spatially distributed sources," *IEEE Trans. Veh Technol.*, vol. 59, no. 3, pp. 1534-1538, 2010.

[7] Boujemâa H, "Extension of COMET algorithm to multiple diffuse source localization in azimuth and elevation," *Eur. Trans. Telecomm.*, vol. 16, no. 6, pp. 557-566, 2004.

[8] L. Cheng, Y. -C. Wu, J. Zhang and L. Liu, "Subspace identification for DOA estimation in massive/full-dimension MIMO systems: bad data mitigation and automatic source enumeration," *IEEE Trans. Signal Process*, vol. 63, no. 22, pp. 5897-5909, 2015.

[9] T. Wu, Z. Deng, X. Hu, A. Li and J. Xu, "DOA estimation of incoherently distributed sources using importance sampling maximum likelihood," *J. Syst. Eng. Electron.*,vol. 33, no. 4, pp. 845-855, 2022.

[10] J. Zhuang, H. Xiong, W. Wang and Z. Chen, "Application of manifold separation to parametric localization for incoherently distributed sources," *IEEE Trans. Signal Process.*, vol. 66, no. 11, pp. 2849-2860, 2018.

[11] S. Shahbazpanahi, S. Valaee and M. H. Bastani, "Distributed source localization using ESPRIT algorithm," *IEEE Trans. Signal Process.*, vol. 49, no. 10, pp. 2169-2178, 2001.

[12] R. Cao, F. Gao and X. Zhang, "An angular parameter estimation method for incoherently distributed sources via generalized shift invariance," *IEEE Trans. Signal Process.*, vol. 64, no. 17, pp. 4493-4503, 2016.

[13] H. Chen, Y. Liu, Q. Wang, W. Liu and G. Wang, "Two-dimensional angular parameter estimation for noncircular incoherently distributed sources based on an L-shaped array," *IEEE Sens. J.*, vol. 20, no. 22, pp. 13704-13715, 2020.

[14] Gu, H. Wang, W. Sun, T. Wu and Y. Xu, "A sequential ESPRIT algorithm based on a novel UCSA configuration for parametric estimation of two-dimensional incoherently distributed source," *IEEE Trans. Veh Technol.*, vol. 70, no. 1, pp. 356-370, Jan. 2021.

[15] Yonghong Liu, Hua Chen, Qing Wang, Wei Liu, Gang Wang, "Noncircularity-based generalized shift invariance for estimation of angular parameters of incoherently distributed sources," *Signal Process.*, vol. 183, pp. 107989, 2021.

[16] Zhi Zheng, Jian Lu, Wen-Qin Wang, Haifen Yang, Shunsheng Zhang, "An efficient method for angular parameter estimation of incoherently distributed sources via beamspace shift invariance," *Digit. Signal Process.*, vol. 83, pp. 261-270, Vol. 2018.

[17] A. Hu, T. Lv, H. Gao, Z. Zhang and S. Yang, "An ESPRIT-based approach for 2-D localization of incoherently distributed sources in massive MIMO systems," *IEEE J. Sel. Topics Signal Process.*, vol. 8, no. 5, pp. 996-1011, 2014.

[18] Z. Zheng, W. -Q. Wang, H. Meng, H. C. So and H. Zhang, "Efficient beamspace-based algorithm for two-dimensional DOA estimation of incoherently distributed sources in massive MIMO systems," *IEEE Trans. Veh Technol.*, vol. 67, no. 12, pp. 11776-11789, 2018.

[19] Tiejun Lv, Fangqing Tan, Hui Gao, Shaoshi Yang, "A beamspace approach for 2-D localization of incoherently distributed sources in massive MIMO systems," *Signal Process.*, vol. 121, pp. 30-45, Vol. 2015.

[20] Hassen S B, Samet A, "An efficient central DOA tracking algorithm for multiple incoherently distributed sources," *EURASIP J. Adv. Signal Process.*, pp. 1-19, 2015.

[21] Wu T, Zhang P, Li Y, "DOA tracking of two-dimensional coherent distribution source based on fast approximated power iteration," *Math. Probl. Eng.*, vol. 1, pp. 3219516, 2020.

[22] He Xu, Ye Tian, Shuai Liu, "Linear-shrinkage-based DOA estimation for coherently distributed sources considering mutual coupling in massive MIMO systems," *Int. J. Electr. Commun.*, vol. 126, pp. 1-6, 2020.

[23] Rao C R, Sastry C R, Zhou B. "Tracking the direction of arrival of multiple moving targets," *IEEE Trans. Signal Process.*, vol. 42, no. 5, pp.1133-1144, 2002.

[24] Wu, Tao, Zhenghong Deng, and Jiwei Xu. "Efficient DOA tracking of two dimensional incoherent distributed sources with double parallel linear arrays," *International Journal of Electronics.*,pp.1781-1802, 2022.

[25] R. P. S. Mahler, "Multitarget Bayes filtering via first-order multitarget moments," *IEEE Trans. Aerosp. Electron. Syst.*, vol. 39, no. 4, pp. 1152-1178, 2003.

[26] R. P. S. Mahler, "PHD filters of higher order in target number," *IEEE Trans. Aerosp. Electron. Syst.*,vol. 43, no. 4, pp. 1523-1543, 2007.

[27] B. -T. Vo, B. -N. Vo and A. Cantoni, "The cardinality balanced multi-target multi-bernoulli filter and its implementations," IEEE Trans. on Signal Processing," *IEEE Trans. Signal Process.*, vol. 57, no. 2, pp. 409-423, 2009.

[28] B. -N. Vo, B. -T. Vo and D. Phung, "Labeled random finite sets and the bayes multi-target tracking filter," *IEEE Trans. Signal Process.*, vol. 62, no. 24, pp. 6554-6567, 2014.

[29] B. -T. Vo and B. -N. Vo, "Labeled random finite sets and multi-object conjugate priors," *IEEE Trans. Signal Process.*, vol. 61, no. 13, pp. 3460-3475, 2013.

[30] S. Reuter, B. -T. Vo, B. -N. Vo and K. Dietmayer, "The labeled multi-bernoulli filter," *IEEE Trans. Signal Process.*, vol. 62, no. 12, pp. 3246-3260, 2014.
[31] B. -N. Vo, B. -T. Vo and H. G. Hoang, "An efficient implementation of the generalized labeled multi-bernoulli filter," *IEEE Trans. Signal Process.*, vol. 65, no. 8, pp. 1975-1987, 2017.
[32] R. P. S. Mahler, B. -T. Vo and B. -N. Vo, "Forward-backward probability hypothesis density smoothing," *IEEE Trans. Aerosp. Electron. Syst.*, vol. 48, no. 1, pp. 707-728, 2012.
[33] Xiangyu He, Guixi Liu, "Improved gaussian mixture probability hypothesis density smoother," *Signal Process.*, vol. 120, pp.56-63, 2016.
[34] S. Nagappa, E. D. Delande, D. E. Clark and J. Houssineau, "A tractable forward– backward CPHD smoother," *IEEE Trans. Aerosp. Electron. Syst.*, vol. 53, no. 1, pp. 201-217, 2017.
[35] M. Beard, B. T. Vo and B. -N. Vo, "Generalised labelled multi-Bernoulli forward-backward smoothing," *in Proc. 19th Int. Conf. Inf. Fusion, Heidelberg, Germany*, 2016, pp. 688-694.
[36] B. -N. Vo and B. -T. Vo, "A multi-scan labeled random finite set model for multi-object state estimation," *IEEE Trans. Signal Process.*, vol. 67, no. 19, pp. 4948-4963, 2019.
[37] Nguyen, Tran Thien Dat, and Du Yong Kim, "GLMB tracker with partial smoothing," *Sensors.*, vol. 19, no. 20, pp. 4419, 2019.
[38] A. S. Rahmathullah, Á. F. García-Fernández and L. Svensson, "Generalized optimal sub-pattern assignment metric," *in Proc. 17th Int. Conf. Inf. Fusion, Xi'an, China*, 2017, pp. 1-8.

Hui Chen received the Ph.D. degree in control science and engineering from Xi'an Jiaotong University, Xi'an, China, in 2016. He is now a Professor in the School of Automation and Electrical Engineering, Lanzhou University of technology, Lanzhou, China. During 2018-2020, he did research on data fusion at the Department of Systems Engineering and Operations Research, George Mason University, Fairfax, VA, USA. His research interests include data fusion, statistical signal processing, random set theory, sensor management, optimal control and intelligent decision-making.

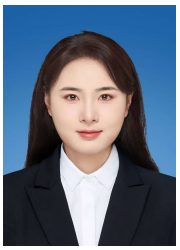

Tianjing Wang received the M.S. degree from Lanzhou University of Technology in 2025. Her research interests include array signal processing, DOA estimation and multi-target tracking.

Wenxu Zhang received the Ph.D. degree in control science from Southwest Jiaotong University in 2018. He is a professor with the School of Automation and Electrical Engineering, Lanzhou University of Technology. His research interests include target tracking and intelligent decision making.

Feng Lian received the Ph.D. degree in control science and engineering from Xi'an Jiaotong University, Xi'an, China, in 2009. He is a Professor with the School of Automation Science and Engineering, Xi'an Jiaotong University. His research interests include multi-source information fusion, filtering and estimation algorithms, random set theory and target tracking and identification methods based on random finite sets, aerodynamic fusion algorithms.

Guanghua Zhang received the B.Eng. degree in automation from China University of Petroleum (East China), Dongying, China, in 2011, and the Ph.D. degree in control science and engineering from Xi'an Jiaotong University, Xi'an, China, in 2018. He is a Professor with Xi'an Jiaotong University. His research interests include target tracking, information fusion, and random finite sets.